Dissipative Solitons in Pattern-forming Nonlinear Optical Systems: Cavity Solitons and Feedback Solitons

Thorsten Ackemann and William J Firth

[1] Institut für Angewandte Physik, Westfälische Wilhelms-Universität Münster, Corrensstraße 2/4, 48149 Münster, Germany, t.ackemann@uni-muenster.de
[2] Department of Physics and Applied Physics, University of Strathclyde, Glasgow G4 0NG, United Kingdom, willie@phys.strath.ac.uk

Many dissipative optical systems support patterns. Dissipative solitons are generally found where a pattern coexists with a stable unpatterned state. We consider such phenomena in driven optical cavities containing a nonlinear medium (cavity solitons) and rather similar phenomena (feedback solitons) where a driven nonlinear optical medium is in front of a single feedback mirror. The history, theory, experimental status, and potential application of such solitons is reviewed.

1 Introduction

Spatial optical solitons are beams of light in which nonlinearity counterbalances diffraction, leading to a robust structure which propagates without change of form (Fig. 1a). These intriguing objects are solutions of nonlinear wave equations. In the conservative case, the range of materials is rather limited – they need to be self-focusing – and in many cases the existence of stable spatial solitons is also limited to one-dimensional systems. Such is the case for the simplest soliton medium, one with a Kerr nonlinearity, i.e. a refractive index which changes in proportion to the intensity of the light. However, as this book demonstrates, in the last years it became increasingly clear that more general schemes can support stable soliton-like solutions with lots of intriguing and new properties, if dissipation and feedback are explicitly introduced. Among these *dissipative solitons*, localized bright spots in driven optical cavities (Fig. 1b, c) received particular attention. They share some properties with spatial solitons, and we will refer to them as *cavity solitons* (CS). Actually, a 'half-cavity' turns out to be enough, i.e. very similar objects are found in arrangements in which feedback is provided by a single-mirror only (Fig. 1d, 'single-mirror feedback scheme'). We will refer to them as *feedback solitons* (FS). Structures such as CS and FS could be natural 'bits' for

parallel processing of optical information, especially since they can be found in semiconductor micro-resonators.

In this chapter we briefly review the history and underlying nonlinear optics of cavity and feedback solitons. We then describe in more detail some models which show these soliton-like structures. It is somewhat paradoxical that stable cavity solitons can exist in media with properties different from, even opposite to, those required for Kerr-medium solitons. We therefore discuss candidate physical interpretations of these structures. We examine the perturbation eigenmodes of CS in sample systems, which give information on the soliton's stability and response to external influences such as noise, neighboring solitons or gradients of the holding field. Cavity solitons can be created by localized pulses of light, and could thus be used to capture and process images or information. The ability to control and manipulate these solitons offers potential advantages over competing systems, and we mention some device ideas which might capitalize on these advantages. These theoretical considerations are supplemented by experimental results, mainly on FS. Finally, we comment on similarities and differences of FS and CS.

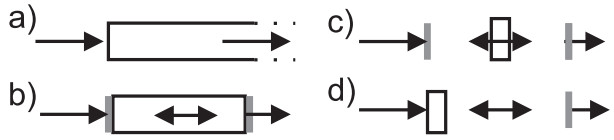

Fig. 1. Nonlinear optical systems supporting pattern formation and solitons (plane mirrors are drawn in grey): a) nonlinear beam propagation, b) cavity filled with nonlinear medium, c) cavity with a short medium, d) single-mirror feedback arrangement.

This article concentrates mainly on the work of ourselves and collaborators. This is primarily for convenience, and serves to illustrate points of general relevance, but we have tried to present a fair and reasonably comprehensive list of relevant references. Further information can be found in earlier reviews and monographies [1, 2, 3, 4, 5, 6, 7, 8, 9, 10]. We mention also a recent feature section on CS in *IEEE Journal of Quantum Electronics* [11]. Additional material on experiments on CS in semiconductor microresonators can be found in the chapter by Taranenko and Weiss [12] in this book. CS in lasers are covered by Rosanov's chapter [13]. There is a rich phenomenology and literature on CS which rely on the coupling of several *optical fields* through, for example, a $\chi^{(2)}$ nonlinearity. This has been shown in mean-field models to support cavity solitons in both second-harmonic-generation (SHG) [14, 15, 16] and optical parametric oscillator (OPO) [17, 18, 19, 20, 21, 22, 23, 24, 25, 26] configurations. Another example is a two-photon laser [27]. A vector Kerr medium also involves coupled fields, and exhibits *polarised* CS for appropriate parameters [28, 29, 26]. Polarized CS exist also in $\chi^{(2)}$-materials [15, 23] and

suitable conditions can be envisaged in certain single-mirror systems [30]. We remark that in these systems CS are often due to a coexistence of two homogeneous states which arise from a symmetry-breaking pitchfork bifurcation. Thus, they are somehow different from the CS on which this review focuses, and to do them justice would have required a substantial lengthening of this article, and so we have chosen not to deal further with these structures, directing the interested reader to the cited literature. Experimental evidence for such structures was given in intra-cavity four-wave mixing [31, 32, 4] and recently in a single-mirror system [33]. Experimental investigations on CS in self-imaging laser schemes and other oscillators are reported in [34, 35, 36, 4].

2 History

The story of cavity solitons probably began with the seminal paper of Moloney and co-workers [37, 38], who used split-step FFT methods to simulate transverse effects in optical bistability (OB) [39, 40]. The model system was a ring cavity, driven by a gaussian beam, and containing a self-focusing Kerr-like medium. The field was propagated (in z) around the cavity, and added coherently to the driving beam at the input beam-splitter. The transverse simulation was one-dimensional (1D), i.e. the intra-cavity field was described by $E_n(x, z)$ with n counting the cavity round-trips. When the input field was ramped up to exceed the OB switch-up threshold, the beam center switched, and a *switching wave* moved out, switching up most of the beam (Fig. 2). Then something unexpected happened: a new instability. The interface between the 'on' and 'off' domains spawned what would now be termed a modulational instability (MI) of the 'on' region, which broke up into a set of distinct peaks [37,38]. These were interpreted as a group of spatial solitons circulating in the medium, perturbed by the output coupling losses and sustained by the input field. Such a physical model has been termed 'soliton-in-a-box' [41]. Such an interpretation is tenable only for a medium which could sustain solitons, and thus cannot be a general model for CS and FS.

In this early cavity soliton work [37, 38] the beam either contains no solitons, or is full of solitons: just two states, and therefore only a one-bit memory in applications terms. McDonald and Firth [42] showed that it was possible to make the individual solitons independently switchable by using a pump beam with a spatially-varying amplitude. They modeled a 20-bit memory of this kind, and also showed that it was possible to switch solitons 'off' as well as 'on' (with an out-of-phase address pulse) [43].

The other key CS pioneer was Rosanov, who from study of OB switching waves developed the idea of 'diffractive autosolitons' [44, 45] in nonlinear optics. Switching waves between co-existent stable states are known in many fields, such as reaction-diffusion systems. Purely diffusive switching waves have monotonic profiles, and the more stable state simply wipes out the less stable, as was shown in an OB model with pure diffusion [46]. When diffraction

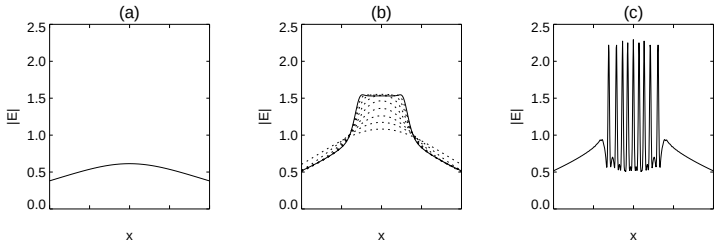

Fig. 2. Gaussian beam switching in an OB cavity. The central section of a smooth broad beam (a) switches; a switching wave then forms and moves out (dotted curves in (b); the high-intensity central region then breaks up into spikes (after Moloney *et al.* [37, 38]).

is present, however, the switching wave typically has ripples. These can trap other switching waves, and thus two can trap each other. Or, in 2D, one switching wave might bend around and close on itself, forming a stable island of one phase surrounded by the other – a diffractive autosoliton (DAS) [44,45]. Here, then, is a second physical interpretation of cavity solitons: self-trapped switching waves. Note that here there is no requirement for bulk solitons: indeed Rosanov showed that DAS can occur even in a saturable absorber. Nor is OB required: even in its absence one can still have switching waves, e.g. between homogeneous and patterned states.

Rosanov has made many significant contributions to OB and related fields on which excellent reviews are available [1, 9]. His work includes also DAS in lasers. The interested reader is referred to these reviews and to Rosanov's chapter in this book [13].

In terms of early experiments, a 1990 special issue of JOSA B [47] gives a useful snapshot and overview of the field. There were pioneering experiments on driven plano-planar resonators containing a liquid-crystal cell [48, 49] published shortly afterwards. Regarding feedback-mirror experiments, as early as 1988 there was experimental evidence of spatio-temporal structure in sodium vapor coupled to a feedback mirror [50], albeit with a long optical path and low Fresnel number.

3 Mean-Field Models and Cavity Solitons

Analysis and modelling of patterns and solitonic phenomena is much simplified in so-called mean-field cavity models, in which alternation of propagation around the cavity with coherent addition of the input field is replaced by a single partial differential equation with a driving term. In the context of spatial pattern formation, this approach is ascribed to the seminal paper of Lugiato and Lefever [51]. Here we give a heuristic derivation of the Lugiato-

Lefever (LL) equation, starting from the well-known Nonlinear Schrödinger Equation (NLS), which describes (conservative) solitons in Kerr media.

The NLS assumes an *infinite* nonlinear medium. Real nonlinear optical media have finite dimensions and (except in glass fibre) solitons can rarely propagate more than a few centimetres before running out of material (Fig. 1a). This perhaps makes it natural to put mirrors around the medium, confining the soliton into a finite slab of material (Fig. 1b). With perfect reflection and zero absorption, one could indeed confine a soliton in such a 'box'. Real mirrors and materials are lossy, but we can make good the loss by 'feeding' the caged soliton with an input field. We are thus led to consider a perturbed NLS:

$$i\frac{\partial E}{\partial t} + \frac{1}{2}\frac{\partial^2 E}{\partial x^2} + |E|^2 E = i\varepsilon(-E - i\theta E + E_{\rm in}) \tag{1}$$

The terms on the left are standard NLS terms, describing respectively evolution, diffraction and (Kerr) nonlinearity. The three terms on the right side are perturbations of the NLS, all small if ε is. The first is just a linear loss ($\varepsilon > 0$), and the last is the driving field $E_{\rm in}$ needed to sustain E against that loss. Less obvious is the middle term, in θ, but we must remember that coherent light confined between mirrors lies within an optical cavity, and so the response to the driving field will strongly depend on whether or not it is in resonance with the cavity. Hence, therefore, the presence of θ, the *cavity mistuning*. If we ignore the *left* side of (1), then $E = E_{\rm in}/(1 + i\theta)$, showing that the cavity has a resonance Lorentzian in θ. This is appropriate for high finesse, where just a single longitudinal mode may be considered.

There is one further change from the usual spatial-soliton NLS: propagation (in z) is replaced by evolution (in t). This is natural: the soliton is now in a box, and not going anywhere.

In the limit $\varepsilon \to 0$ equation (1) recovers the NLS, with a soliton solution of sech-profile in x, time independent except for a phase rotation. We might expect, therefore, that for finite ε it has sech-like *cavity soliton* solutions for suitable $E_{\rm in}$, and indeed it has. It is usual to consider $E_{\rm in}$ to be a plane wave, independent of x (and y in 2D), in which case the soliton sits on a homogeneous non-zero background field being a solution of (1). A finite but relatively broad driving beam supports cavity solitons qualitatively similar to those predicted for the simpler plane-wave input case. We remark that (1) is not the only possible dissipative version of the NLS which might be envisaged. For example, in [52] a damped and parametrically driven version of the NLS is considered which serves as a model for 'oscillons', 2D localized states in shaken granular materials [53]. They can be regarded as another manifestation of dissipative solitons.

We now set $\varepsilon = 1$, which is equivalent to a re-scaling. This yields the Lugiato-Lefever (LL) equation, which was originally introduced [51] as a model for pattern formation. Note that in the LL equation time t is scaled to the cavity loss time. The NLS limit is recovered as $\theta \to \infty$. The LL equation

is also appropriate as a mean-field model for OB with transverse effects. The term 'mean-field' arises because such models are usually derived by assuming a high finesse, so that the cavity field is approximately constant along the cavity axis. The high finesse allows the Airy function response of the cavity to be approximated by a single longitudinal mode, giving the Lorentzian resonance mentioned above. For a plane-wave pump, the plane-wave cavity field obeys $E_0 = E_{\rm in}/[1+i(\theta-|E_0|^2)]$, which is three-valued for $\theta \geq \sqrt{3}$, showing that the model exhibits OB [51]. In fact, Lugiato and Lefever showed that E_0 is stable if $|E_0| < 1$, but unstable, usually because of spontaneous pattern formation, above that threshold [51]. In truth Fig. 2 was generated by simulating the LL equation (for $\theta = 2.1$, $E_{\rm in} = 1.5$ for *(a)* and 2.5 for *(b)* and *(c)*), rather than the original model of Moloney *et al.* [37,38]. The strong similarity of the respective results shows how such mean-field models can capture the essential features of a full cavity model while being both cheaper to simulate and easier to analyze.

Such analysis is still by no means simple. Unlike for the NLS, no exact analytical solutions for patterns or solitons are known for the LL equation. The usual approach has been to perturbatively derive amplitude equations or to resort to numerical integration of the model, neither of which is ideal. Perturbative approaches, by their very nature, cannot provide quantitative results and integration gives a very restricted view of the model's bifurcation behavior, by only finding solutions which are dynamically stable. Another technique, which we have used extensively [41,54,55,56,57] is to use numerical methods to find the system's stationary solutions, their stability and their response to perturbations. We will first apply the method to the LL equation and later to other CS and FS models.

We look for stationary solutions ($\partial/\partial t = 0$) of equation (1), after setting $\varepsilon = 1$ as discussed:

$$0 = -(1 + i\theta)E + i|E|^2E + i\Delta_\perp E + E_{\rm in} \tag{2}$$

where the exact form for the transverse Laplacian $\Delta_\perp$ depends on whether we consider 1D, cylindrically symmetric, or fully 2D geometries. We discretize the space variable(s) on N grid points, apply periodic boundary conditions and use a Fast Fourier Transform (FFT) algorithm to evaluate the spatial derivatives. This gives a highly accurate, $O(N)$, set of coupled algebraic equations which can be solved using an iterative Newton method. Given a suitably close initial guess, this method rapidly converges to a stationary solution (not necessarily a stable one) of the original LL equation. These solutions can then be tracked in parameter space, tracing out branches.

The use of a Newton method is advantageous because, as a by-product of this process, it also finds the linearization, in the form of a Jacobian matrix, around the solution found. The resultant eigenvalues, β, give the solutions' stability and the eigenvectors $\{\mathbf{u}\}$ the associated modes.

Fig. 3 shows three solution branches tracked in this way. The lower line shows the plane-wave solution discussed already to be stable below $|E_0|^2 = 1$

and unstable above. At this point, a branch of localized, cylindrically symmetric ($\nabla^2 = \partial^2/\partial r^2 + 1/r\partial/\partial r$) solutions bifurcates subcritically before bending around to form a positive-slope branch of finite amplitude. This upper branch is the cavity equivalent of the unstable soliton-like solution to the 2D NLS. This bifurcation structure is typical of cavity solitons in many systems. For values of $|E_{\rm in}| > E_{\rm in}^{(\rm sn)}$ the two branches co-exist with the homogeneous background, to which the solitons asymptote at large radius. Note that only for $\theta > \sqrt{3}$ the homogeneous solution is multi-valued and so, over a broad range, any interpretation of CS as self-trapped switching waves must relate to the interface between the homogenous solution and a pattern, rather than simply between homogeneous solutions. We will discuss the relationship between patterns and CS in some detail below.

We now turn to the stability of these cavity soliton solutions. As might be expected, the lower branch of the loop is always unstable but, unlike the 2D NLS case, the upper branch may be stable [58]. The solid portion of the upper branch in Fig. 3 shows where they are stable. We find that the onset of instability is due to the presence of a Hopf bifurcation [58, 59], not, as in bulk Kerr media, collapse. Direct simulation confirms the stability analysis. A perturbed cavity soliton exhibits damped oscillations in the stable domain, which become undamped as the stability boundary is crossed. Inside the instability region, the CS shows periodic oscillations, but still does not collapse, even well beyond threshold. Instead its minimum-amplitude shape becomes very similar to that of the unstable CS solution belonging to the lower branch in Fig. 3. Because that solution has only one unstable eigenmode, it acts as a quasi-attractor for the oscillating CS, which dwells close to it before eventually moving away along its unstable manifold [59].

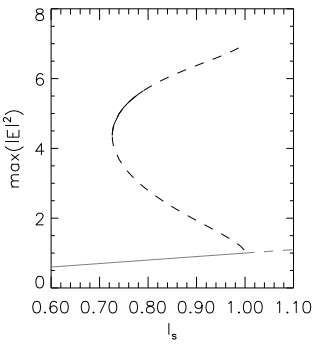

Fig. 3. Branches showing the homogeneous solution and the cylindrically symmetric cavity soliton solution for the 2D Kerr cavity, as a function of the background intracavity intensity $I_{\rm s} = |E_0|^2$. Solid curves indicate stable solutions, dashed unstable ($\theta = 1.3$).

The stability of 2D cavity solitons in the Lugiato-Lefever mean-field model is a behavior qualitatively different from its bulk-medium equivalent. This encourages exploration of other models which might support CS. Comparing the LL equation with the NLS, we note that the diffraction term and the nonlinearity are not specifically associated with the cavity. We already modified the diffraction term when we considered the 2D Kerr cavity. We can go further and add *dispersion* to make '3D' cavity solitons [60, 61]. Or we can replace diffraction with dispersion, and consider e.g. fibre cavities, where Mitschke and co-workers [62] have found evidence of soliton-like structures in synchronously-pumped fibre loops, and Wabnitz [63] has examined data storage issues. This case is equivalent to diffraction in the 1D geometry of the LL equation, and the existence and stability of CS in 1D is perhaps to be expected.

The nonlinearity also offers considerable scope for variation. Perhaps the obvious generalization from the Kerr nonlinearity is to a two-level atom-like response, which becomes Kerr-like far from the atomic resonance. For exact atomic resonance the medium is just a saturable absorber, with no nonlinear refractive index contribution. It nonetheless supports stable, robust cavity solitons [45, 64, 65].

The simplicity of the saturable absorber makes it a very useful model for CS investigations, and we will use it as illustration of some interesting and general CS phenomena. The spatio-temporal dynamics of the slowly varying amplitude of the electromagnetic field E is modeled by

$$\partial_t E = -E\left(1 + i\theta + \frac{2C}{1+|E|^2}\right) + i\Delta_\perp E + E_{\rm in}, \tag{3}$$

which differs from the Kerr cavity equation (1) only in the nonlinear term, in which C is a scaled atomic density. Since C is real and positive, this a purely dissipative term, which in fact describes the linear as well as nonlinear absorption due to the medium. The field scaling is such that the saturation intensity of the transition corresponds to $|E| = 1$.

The homogeneous solution E_0 of this equation (with plane-wave $E_{\rm in}$) can be multi-valued if $C > 4$ (absorptive OB). With or without OB, it can become unstable to pattern formation [66], where the wave-vector K of the pattern at threshold is simply given by $K^2 = -\theta$. This obviously requires that the cavity mistuning θ be negative or, in physical terms, that the frequency (and the corresponding wave vector, of course) of the intra-cavity field is higher than the frequency (and wave vector) of the longitudinal (i.e. the on-axis) resonance of the cavity. This has a simple physical interpretation - the unstable mode is off-axis by just enough to compensate for the cavity mistuning, so that this is a so-called 'tilted-wave' instability.

Figure 4 gives a demonstration of this scaling behavior. The panels a) and b) display the near field intensity distributions observed in a vertical-cavity regenerative amplifier driven electrically above transparency but below the

self-oscillation threshold (Fig. 1c, [67]). Though the injected external optical field is a smooth on-axis wave, the output shows spontaneous patterning and the scale of the pattern depends on the frequency of the injected field which defines also the oscillation frequency of the intra-cavity field. The patterns become coarser as the injection wave length approaches the longitudinal cavity resonance, as expected from the above consideration. The data depicted in panel c) demonstrate also very nicely that indeed the square of the transverse wave vector depends linearly on detuning. We note that the simple scaling between the empty cavity detuning and the transverse wave vector holds only for purely absorptive media. In dispersive media (in particular in semiconductor media), the shift in resonance due to the nonlinear refractive index shift induced by the background field needs to be taken into account.

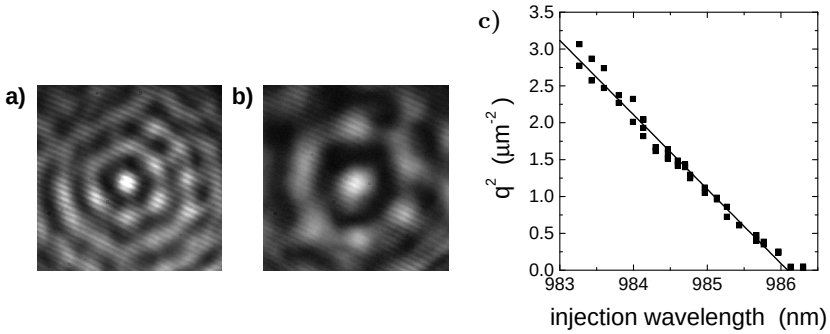

Fig. 4. a,b) Near field intensity distribution observed in a vertical cavity regenerative amplifier for an injection detuned by about (a) 1.1 nm and (b) 0.4 nm. c) Square of transverse wavevector in dependence on the injection wavelength (adapted from [67]).

We dwelt on this issue in some detail because it will become clear when we discuss the connection between CS and patterns, and in particular the 'pattern element' interpretation of CS, that the scaling properties of the pattern wavelength carry over to the half width of CS and to the minimum allowed distance between them, at least to a great extent. Of course a soliton parameter such as the half width is also affected by diffusion, nonlinearity etc. We remark that such a scaling is a general feature of optical pattern forming systems, since it is a direct consequence of the scaling properties of the paraxial wave equation.

CS in the absorptive model (3) have recently been examined in detail in [56]. We show in Fig. 5 a range of such solutions, including not only simple single-peaked CS, but multi-peaked localized solutions in which up to four similar-sized peaks sit on a flat background. The latter four-peak structure invites interpretation as an 'island' of pattern set in the homogeneous solution (which is single-valued for these parameters), an interpretation which we will

now examine. We should first note that these CS solutions are presented in terms of $A(x)$, where by definition $E = E_0(1 + A)$, so that in terms of A localized solutions sit on a zero background. Second, note that for any given input field, all the peaks in these solutions seem to have one of two heights. In particular, there are two single-peak CS of different amplitudes. This is general - the low-amplitude-peak belongs to a branch of unstable CS which bifurcates subcritically from the homogeneous solution at the pattern-formation threshold [65,56], before bending back in a saddle-node bifurcation to become the high-amplitude-peak branch (which is stable). The Kerr CS discussed show a similar bifurcation structure (see Fig. 3).

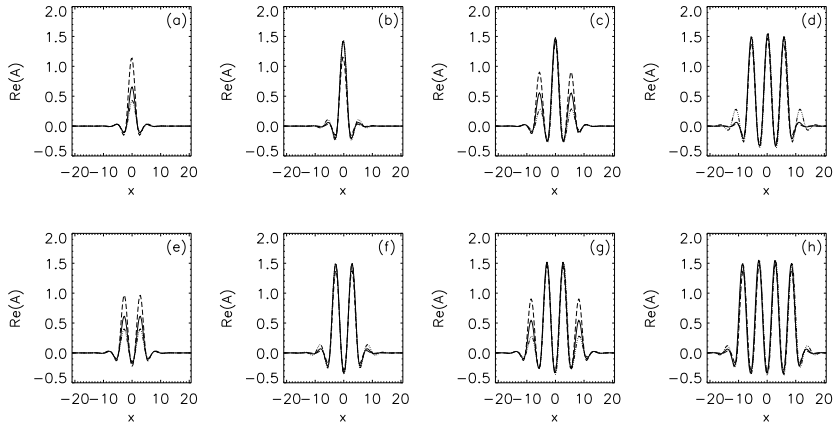

Fig. 5. Sequences of profiles of one-dimensional CS solutions to equation (3) with respectively odd (above) and even (below) numbers of main peaks. Dash-dotted, solid and dashed lines correspond to solutions at $|E_0|^2 = 1.22$, $|E_0|^2 = 1.33$ and $|E_0|^2 = 1.44$. Other parameters are $\theta = -1.2$ and $C = 5.4$.

Coullet et al [68,69] have recently offered a general mathematical analysis of this scenario. They consider a situation in which a stable infinite pattern co-exists with a stable homogenous solution. Then one can envisage a configuration in which there is a domain with a pattern and a homogeneous domain, with a *front* at their interface. In general one would expect one or other solution to dominate, such that the front would move, annihilating the weaker solution, until the entire space is filled with the dominant state. One might expect there to be a kind of 'Maxwell point' in parameter space, at which the dominant role switches from the pattern to the homogeneous state or vice versa. In fact Pomeau showed that, because motion of the front requires creation or annihilation of pattern cells, the Maxwell point spreads out into a *locking range* of finite width, within which the front is stationary, i.e. the two states can stably coexist in real space as well as in parameter space [70]. Coul-

let *et al.* showed, using generic properties of ordinary differential equations, that in parameter space such a locking range is always accompanied by an infinite sequence of localized states. As one enters the locking range from the homogeneous-dominant side, pairs of N-peaked states appear in decreasing order of N, while as one exits the range on the pattern-dominant side, these states disappear in order, with the $N = 1$ states surviving longest.

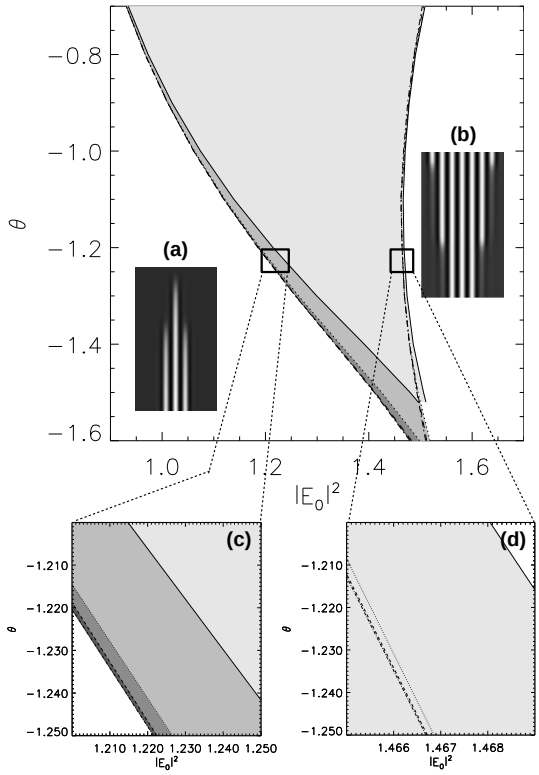

Fig. 6. Existence limits of N-peaked CS structures (shaded regions) in two-dimensional parameter space $(|E_0|^2, \theta)$. Structures with $N = 1, 2, 3, 4$ respectively exist between solid, dotted, dashed and dash-dotted lines. Panels (a) and (b) show space-time plots of unlocking behavior, with the transverse coordinate (x) on the horizontal axis and time (t) on the vertical axis. Panel (c) shows the fine structure of the locking domain, indicated by the square on the main figure. Parameters: $C = 5.4$.

The saturable-absorber CS model (3) in one transverse dimension falls within the class of models to which the Coullet *et al.* theory is relevant, and Fig. 5 is fully consistent with that scenario. McSloy *et al.* [56] used the stationary-solution approach described above to map out the existence domains of the $N = 1$ to $N = 4$ peaked CS solutions in both one and two

dimensions, as a function of the *two* parameters θ and $|E_0|^2$. The results are shown in Fig. 6, and are fully consistent with the analysis of Coullet *et al.* [68,69]. In the broad central region of this figure, there is a stable N-peaked localized state (or multi-CS) for any N. (In practice, N will be limited by the size of the holding beam E_{in} relative to the size of the single-peaked CS.) The analysis used by Coullet *et al.* is not extensible to two transverse dimensions, but in Fig. 7 we show that basically the same phenomena occur [56]. In 2D, multiple peaks transform into clusters, bound states of simple, cylindrically-symmetric, CS [71]. Large clusters, especially symmetric ones, are also referred to as 'localized patterns' [64]. In Fig. 7 we plot the existence domains of single CS, and of dipole, triangular, and rhomboidal clusters [56]. In terms both of parameter ranges, and of succession, these 2D CS structures are qualitatively similar to the better-understood 1D scenario. Also shown are plots of the dynamics of the interesting centered-hexagon ($N = 7$) cluster outside the locking range. It 'dies' in the left-hand (homogeneous-dominant) region, but grows to form a full hexagonal pattern in the right-hand (pattern-dominant) region.

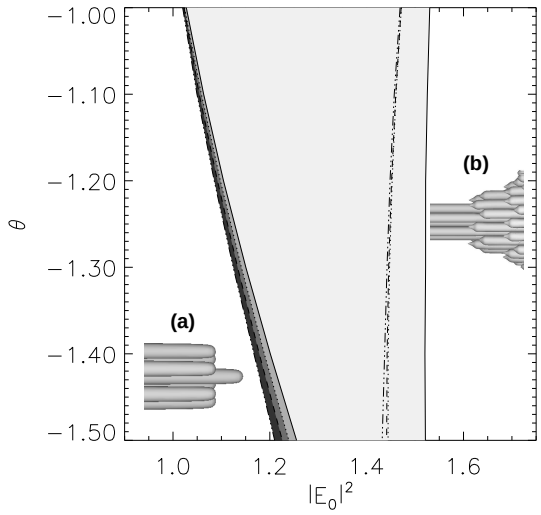

Fig. 7. Locking regimes of 2D *CS* (solid/light gray), and of clusters of two(dotted/gray), three (dashed/dark gray) and four (dot-dashed/black) close-packed clusters of CS with respective existence indicated by (line style / fill shade) ($C = 5.4$). Panels (a) and (b) show the dynamics of a centered hexagon structure ($N = 7$) outside the locking range. Respective intra-cavity field intensities are $|E_0|^2 = 1.08$ and 1.45 with $\theta = -1.2$ and $C = 5.4$.

From this analysis we can conclude that with an appropriate choice of system and parameters we can impress any number of CS up to some aperture-delimited maximum N_{max} on to the output beam of a driven optical cavity

containing a suitable nonlinear medium. Such a medium acts as an N_{max}-state memory, assuming that we can create N-clusters of CS with N appropriately-aimed address pulses. We can do better, however (and need to, if such a CS memory is to be economic). Suppose that each of the component CS making up the N_{max} cluster can be independently switched, by selective addressing at the site of each. Then each site acts as a *pixel*, which is 'on' when it supports a CS, and 'off' when no CS is present at that site. In such a case, we have $2^{N_{max}}$ co-existent states. Some years ago Firth [72] showed that there is a certain equivalence between the condition for the existence of a full set of 2^N coexistent states in a 1D array and the 'Smale horseshoe' condition for dynamical chaos. Though he used a simpler model than Coullet *et al.* [68, 69, 73] (an imposed, not spontaneous, pattern), it seems likely that an analogous development of their approach to consider quasi-random pixel-type patterns will lead to a similar conclusion.

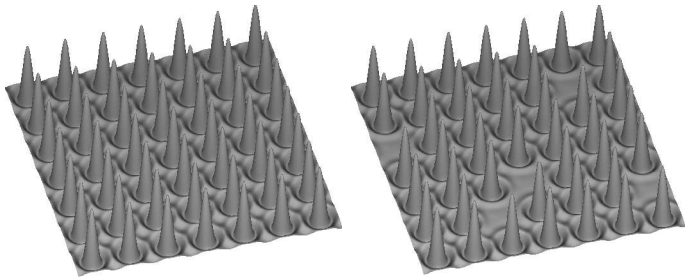

Fig. 8. Regular *vs* irregular patterns. On the left, a 7×7 square pattern. On the right, the same template, but with five of the peaks (i.e. five individual CS) missing. Both arrays are stable. Assuming that, similarly, any or all of the 49 peaks may be present or absent, there are 2^{49} different co-existent stable states of this array. (Optical cavity with saturable absorber: $\theta = -1.2$ and $C = 5.4$.)

Figure 8 illustrates that this idea can work in practice. Using periodic boundary conditions, a stable square 'pattern' exists, as illustrated in the left panel. That this 'pattern' can be regarded as an array of independent CS is illustrated in the right panel, where five of the 'CS' are missing. This structure is also stable, and indeed this array operates in all respects as a 49-bit pixel array memory, in which the pixel is 'on' or 'off' according to whether or not there is a CS at the pixel site.

Given that CS are found in both Kerr and saturable absorber media, it may be no surprise that the intermediate case of a two-level atomic response, with mixed absorptive-dispersive nonlinearity, also supports cavity solitons, though more readily on the self-focusing side of resonance [44,64,74,75,76,77]. It was also shown that these models reduce in some limit to Swift-Hohenberg-like models [78, 64, 74, 66], a generic class of models in spontaneous pattern

formation [79]. An experimental observation of dissipative Kerr-solitons was recently reported for a nonlinear cavity filled with a liquid crystal [80].

A further CS generalization is to consider a nonlinearity mediated by a material excitation. This opens up the further possibility that the medium can have its own dynamics and spatial (usually diffusive) coupling. Semiconductors are particularly interesting among such media, and it has been shown [76,77,81,54,82,83] that cavity solitons extend to semiconductor models, even in the presence of such 'soliton-antagonistic' effects as diffusion and a measure of self-defocusing. Perhaps even more surprisingly, Michaelis *et al.* [84] found bright solitons in a cavity model with a purely-defocusing, diffusive saturable Kerr medium, such as is found in semiconductors just below the band edge. Experimental observations of CS in semiconductor microcavities were reported in [85,86,87,88,89].

4 Self-Propelled Cavity Solitons in Semiconductor Microresonators

Since basic properties of CS in semiconductor microresonators are covered in another chapter of this book [12] and in [86,90], we will concentrate here on an interesting phenomenon which arises when thermal effects are coupled to the light-carrier interaction equations.

Recent papers [92,91] demonstrated and analyzed the existence of both bright and dark spontaneously moving CS in a model of a semiconductor microcavity. The motion is caused by temperature–induced changes in the cavity detuning and arises through an instability of the stationary soliton solution when the temperature-tuning coupling is strong enough. The experimental relevance of this coupling is demonstrated by the observation of opto-thermal pulsations in semiconductor amplifiers [93]. Here, we briefly summarize the main features of these phenomena, and detail just a few interesting examples. More details of the phenomena and of models for CS in semiconductor cavities can be found in [92,91,82] and references therein.

Before describing the particular model to be looked at, a brief digression on the dynamics of CS is indicated. When the driving field is plane–wave and the system invariant with respect to spatial translations, a given stable CS can exist at any location. This symmetry property is manifest in the eigenvalue spectrum of the soliton (or any stable stationary solution) by the fact that there is a marginal mode with eigenvalue zero, which is connected to the translational degree of freedom. All other eigenvalues than this neutral mode $\mathbf{u}_0$ have negative real part, by virtue of the stability of the CS. This means that, as $t \to \infty$, the amplitude a_0 of the neutral mode dominates over all other a_i. Thus the dynamical effect of any perturbation $\boldsymbol{\mathcal{P}}$ on a stationary stable state is primarily determined by its projection onto the neutral mode, which yields the equation [54]:

$$\frac{\mathrm{d}a_0}{\mathrm{d}t} = \frac{1}{< \mathbf{v}_0 \mid \mathbf{u}_0 >} < \mathbf{v}_0 \mid \boldsymbol{\mathcal{P}} > \tag{4}$$

Here $\mathbf{v}_0$ is neutral mode of the corresponding adjoint problem. Because the neutral mode is just the gradient of the CS, physically $\mathrm{d}a_0/\mathrm{d}t$ is the translational velocity of the CS under the influence of the perturbation. Obviously the motion of a such a CS under the influence of an external force is not Newtonian, but overdamped (Aristotelian). Among the various types of perturbation, three of particular relevance are a phase or amplitude gradient of the driving field [65, 1, 54], and perturbation of one soliton by another (see Sec. 7.1). In the case of a weak phase gradient the input field around a CS at $x = 0$ can be locally approximated by $E_{\mathrm{in}} = E_{0,\mathrm{in}}(1 + ikx)$. Inserting the perturbation part $ikxE_{0,\mathrm{in}}$ into (4) we can calculate the drift velocity of a cavity soliton due to the phase gradient (or, similarly, an amplitude gradient) [54].

By turning a parameter (here, the detuning) into a *dynamical variable* by coupling it to the temperature, a spontaneous transition from stationary to moving solitons becomes possible. We note that the stationary-to-moving CS bifurcation has similarities with the Ising–Bloch transition for *fronts* studied in [94] and more recently in [95, 96]. One particularly interesting feature to emerge is that the spontaneously moving CS have *inertia*, so that their dynamics is quasi-Newtonian. In particular, they can rebound from obstacles (or each other), and can oscillate in a potential well, impossible for Aristotelian particles.

The system under consideration is a semiconductor microcavity (Figure 1c) consisting of a thin active region sandwiched between two high reflectivity ($\sim$ 99.9%) distributed Bragg reflectors (DBR). The device can be driven by an external pump field E_{in} and, optionally, an external current J (see [67, 86, 85, 12]). We will concentrate on the case $J = 0$, the so-called passive system [82]. The intra-cavity electric field E, carrier density N and temperature difference T between the lattice temperature and the ambient temperature can be described by the following set of partial differential equations [77, 82, 92, 91]:

$$\frac{\partial E}{\partial t} = -(1 + i\Theta)E + i\Xi\chi E + E_{\mathrm{in}} + i\Delta_\perp E \tag{5}$$

$$\frac{\partial N}{\partial t} = -\gamma_N \Big(N + \beta N^2 - J + (N-1)|E|^2 - D_N \Delta_\perp N \Big) \tag{6}$$

$$\frac{\partial T}{\partial t} = -\gamma_T \Big(T - ZN - PJ^2 - D_T \Delta_\perp T \Big) \tag{7}$$

where $\Delta_\perp$ is the transverse Laplacian in 2D. The strength of the material nonlinearity is parameterized by Ξ. The cavity detuning is denoted by Θ where

$$\Theta = \theta - \alpha T \tag{8}$$

Here θ is the cavity detuning at ambient temperature and α a coupling parameter [97]. Note that if $\alpha = 0$ there is no feedback from heating to the carrier-field dynamics. Thus Equation (8) is the driver of the motional instability, because it embodies the most important consequence of heating in semiconductor microcavity devices: namely, a change in the linear refractive index of the semiconductor material and hence a shift in the cavity resonances [97, 89]. It is thus to be expected that α is the key parameter in the analysis of this instability [91].

Elsewhere in these equations, the term βN^2 describes radiative carrier recombination, carrier and thermal diffusion coefficients [98] are denoted by D_N and D_T, the term ZN describes heating due to nonradiative recombination, and PJ^2 Joule heating by the current (if present).

For the passive MQW device model, the nonlinear susceptibility χ is assumed to be simply a linear function of the carrier density [91]:

$$\chi = \frac{-(\Delta + i)(N - 1)}{1 + \Delta^2} \tag{9}$$

The parameter Δ represents the band-gap detuning.

Finally, the cavity field decays on a time scale of $\tau \approx 10$ ps. This value is used to scale time in Eqs. (5)-(7). Then, the (normalized) time scale for N and T are $\gamma_N^{-1} \approx 100$ and $\gamma_T^{-1} \sim 10^5$, respectively.

Equations (5)-(7) are known to exhibit plane-wave bistability and to possess stable, stationary CS solutions in the absence of thermal effects ($\alpha = 0$) [54]. We are going to describe structures whose existence is due entirely to the effect of temperature changes on the cavity and thereby on the intra-cavity field. In the passive system, the instability to moving solutions is observed for *dark* solitons.

As intensity minima sitting on a high intensity background, dark solitons are expected to exist on the upper branch of the plane–wave bistability curve. Figure 9 shows an example of a dark soliton branch along with plane–wave and roll (stripe) solutions. This particular roll solution has a wavevector $K \simeq 1.3K_c$ where K_c is the most unstable wavevector at the modulational instability threshold. The homogeneous background field shows the underlying plane–wave bistability. For these parameters, dark solitons exist for $5.542 < E_{\rm in} < 5.560$ but are always unstable to spontaneous motion.

An example of a moving dark soliton is given in Figure 10. The physical mechanism is reasonably simple. A stationary dark CS is a region of low intensity, and thus of weak heating, and hence is relatively cold. If the coupling α is positive, that means that the cavity tuning is locally (even) more negative. Without thermal coupling, a CS will move to regions of smaller (absolute) detuning, and so any small displacement of the CS field minimum ('dark spot') from the temperature minimum ('cool spot') will induce it to move further out of the temperature dip, at a speed related to the tuning gradient. This movement is counteracted by the coupling of the temperature to the field and carrier density, which will cause the 'cool spot' to follow the 'dark spot'.

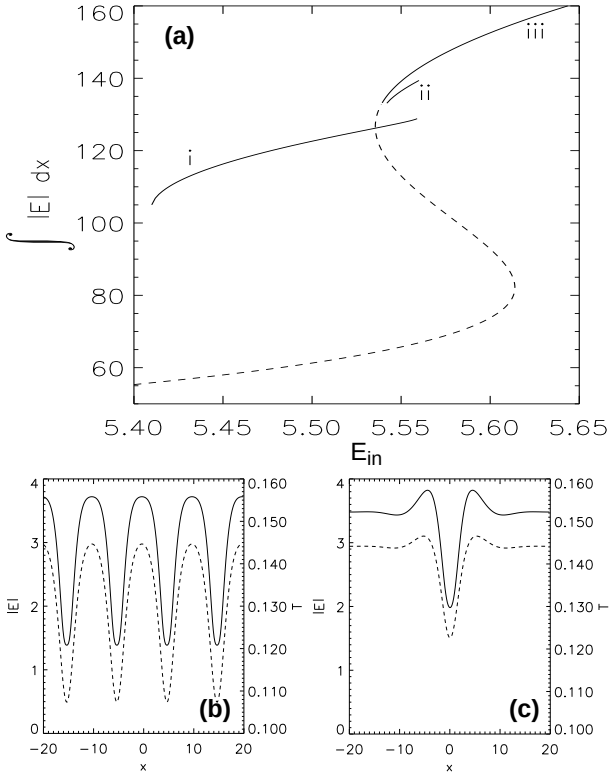

Fig. 9. (a) Solution branches for (i) rolls with $K \simeq 1.3K_c$ and (ii) stationary dark CS. Panels (b) and (c) correspond respectively to points on branches (i) and (ii). Solid and dashed lines respectively denote $|E|$ and T. The homogeneous solution (iii) is stable on solid parts of the curve and modulationally unstable in the dashed region. Parameters are $\alpha = 1$, $D_N = 0.2$, $D_T = 1$, $\gamma_N = 10^{-2}$, $\gamma_T = 10^{-5}$, $\Delta = 10$, $\theta = 0.3$, $\Xi = 80$, $\beta = 1.6$, $Z = 0.172$. (b) $E_{\rm in} = 5.45$ and (c) $E_{\rm in} = 5.55$.

If α is small enough, the dark spot will move only slowly, and the temperature will be able to follow any movement of the other fields, and so the CS will be stable against fluctuations. For larger α, however, the dark spot will move faster, and at some point the slow thermal dynamics will prevent the cool spot from keeping up with the dark spot: then there is a transition to a dynamic equilibrium, in which the CS moves at constant speed. The moving CS is asymmetric, with the dark spot 'ahead' of the cool spot, and so always seeing a tuning gradient. The E and T profiles of a typical moving dark soliton are shown in Figure 10.

One can perform a weakly nonlinear analysis near the bifurcation point between the stationary and moving solutions [91]. The calculation has similarities to that reported in [96]. Omitting mathematical detail, the result is an equation for the velocity of the moving CS which takes the form:

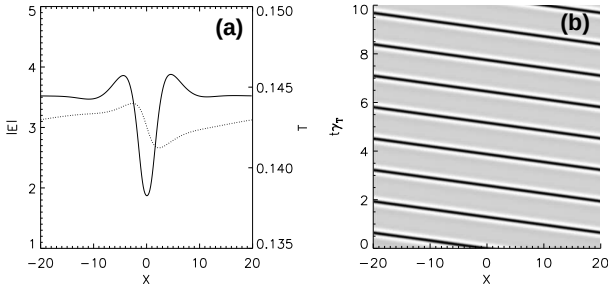

Fig. 10. (a) Magnitude of electric field (solid line) and temperature (dotted line) for a dark, moving CS. (b) Space-time plot of $|E|$ for a moving CS (periodic boundary conditions). Parameters are $E_{\rm in} = 5.39$ and $\alpha = 1$. All other parameters as in Figure 9.

$$\partial_t v = av + bv^3. \tag{10}$$

The linear and cubic coefficients a and b in Equation (10) are constants which can be determined from the CS solution to the field equations. If they are of the same sign, then $v = 0$ is the only stationary solution, but if they are of opposite sign there are also two constant-velocity solutions $v = \pm\sqrt{-a/b}$. This is typical of a pitchfork bifurcation, with the $v = 0$ solution becoming unstable when a changes sign. Figure 11 shows a comparison [91] between the speed predicted by this analysis and the results from numerical simulations of Equations (5)– (7). The agreement is quite good, even more than three times above threshold.

Note that Equation (10) involves the second derivative with respect to time of the CS position, i.e. its acceleration. There is thus a superficial resemblance to a Newtonian force law obeyed by a massive particle. This inertial dynamics is in complete contrast with that of a normally stationary CS. An external perturbation drives the velocity of an otherwise stable stationary soliton, while it drives the acceleration of a spontaneously moving soliton. The latter acquires mass (or rather inertia) because, in essence, the mode which becomes unstable at the bifurcation is *identical* to the neutral mode, giving the CS an extra degree of dynamical freedom [96,91]. (Note that DAS in lasers also obey a quasi-Newtonian equation of motion [1].)

Figure 12 illustrates the inertia effect in the collision of two self–moving CS in two dimensions. They collide and merge, with the outgoing CS traveling in a direction which, at first glance, looks like that of the mass-center of the incoming CS. One must recall, however, that here there is no 'conservation of mass', because the outgoing CS is identical to each of the incoming ones. Nor is there conservation of momentum, in the Newtonian sense, because the *speed* of the outgoing CS is the same of that of the incoming ones, regardless of their directions of motion.

In summary, we have illustrated the existence, in both one and two spatial dimensions, of spontaneously moving cavity solitons in a model of a semi-

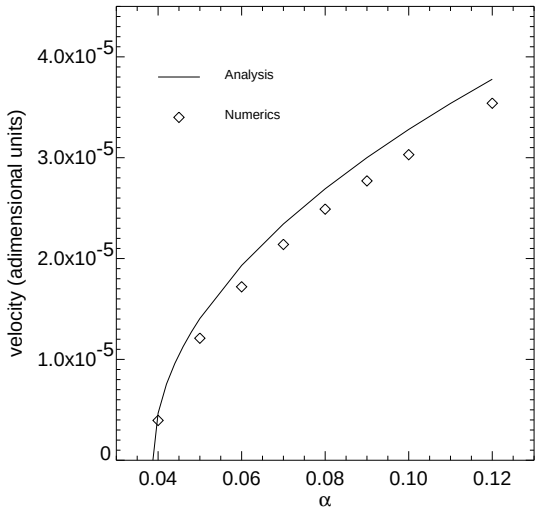

Fig. 11. The velocity of a moving soliton as a function of α: the diamonds indicate results from numerical simulations, while the solid line comes from weakly nonlinear analysis [91].

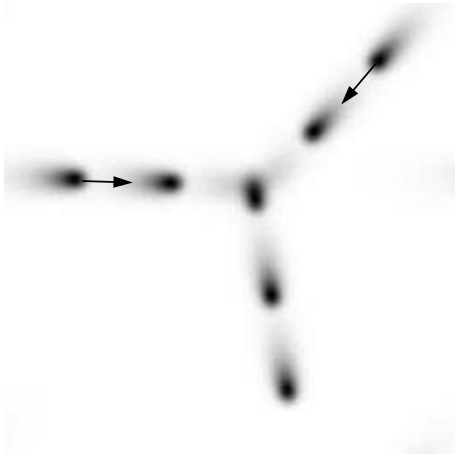

Fig. 12. "Stroboscopic" images of collision and merging of two 2D spontaneously-moving dark CS, showing inertial effects. Arrows indicate initial direction of motion. Shown is the temperature field, obtained in a simplified semiconductor CS model, in which the carrier dynamics is adiabatically eliminated (Eqs. (21,22) of [91]). *Courtesy A. J. Scroggie.*

conductor microcavity. These solitons appear through an instability of the stationary solitons arising from localized cavity tuning variations coupled to temperature changes in the semiconductor induced by the light-carrier interaction. Regardless of the details of the present system, the essential ingredients

appear to be the existence of stationary soliton solutions and the spontaneous creation of self-sustained parameter gradients. Thus similar phenomena should occur in a variety of optical and other systems. Indeed, spontaneously moving dissipative solitons are found in reaction-diffusion models [99] and were recently identified experimentally in gas discharge systems [100].

5 Solitons in a single-mirror feedback arrangement

In the preceding sections, it became evident that dissipative solitons are a robust feature of nonlinear cavities if they are operated close to a pattern-forming instability. In addition, in many cases the existence of CS was accompanied by bistability between plane-wave states, though this was not absolutely necessary. Hence it appears to be natural to look for solitons also in other nonlinear optical systems allowing for pattern-formation and/or optical bistability. In the context of pattern formation, the so-called 'single-mirror feedback scheme' [101, 102, 103, 6] has emerged as an experimental and theoretical workhorse for studying complex self-organization behavior in space and time and hence it is maybe not too surprising that dissipative solitons can be also found in these systems [104, 105, 106, 107, 108, 109, 110, 111, 112, 113, 114, 115, 116].

5.1 Single-mirror feedback arrangements: Mechanism of spatial instability

The basic scheme discussed in the following is depicted in Fig. 1d. It is a thin slice of a nonlinear medium irradiated by a spatially smooth beam (ideally a plane wave with uniform amplitude and phase). A plane feedback mirror is placed at a distance d after the medium to generate a counter-propagating beam in the nonlinear medium [101, 102, 103]. The basic idea in the idealized scheme is the spatial separation of the region in which nonlinearities are at work and the region in which diffraction takes place: If the slice is sufficiently thin, propagation in the slice can be neglected and it will provide just some phase modulation and amplitude modulation. In this way the theoretical treatment is tremendously simplified.

Now consider a weak perturbation in the form of a sinusoidal modulation of the index of refraction in a dispersive nonlinear medium, e.g. a Kerr medium. This modulation will give rise to a weak phase modulation of the transmitted wave. Diffraction during the propagation to the mirror and back will usually convert phase modulation, at least partially, into amplitude modulation. However, in a Kerr medium an amplitude modulation generates a corresponding index modulation, and so the original fluctuation can be enhanced and sustained by positive feedback. The connection between the longitudinal and transverse length scales at which conversion between phase and amplitude

modulation takes place is given by the paraxial wave equation. The phase of an off-axis wave with transverse wave vector K evolves like

$$\phi = \frac{iK^2 z}{2k_0} \tag{11}$$

after propagation over a distance z (k_0 wave vector of light). The periodicity of the phase in (11) in dependency on z is also at the heart of the so-called Talbot-effect [117, 118], i.e. the periodic recurrence of amplitude and phase modulation along the propagation direction. Eq. (11) implies that for a given phase shift the selected wave length scales with the square root of the mirror distance d [101,102,103,6]. Note the similarity to the cavity case: both schemes rely on the differences in phase shift acquired during propagation for different tilt angles. However, in the cavity it is the interference condition provided by the cavity boundary conditions which converts the accumulated phase into amplitude, whereas here it is the interference of the off-axis wave with the on-axis carrier.

For a 'dynamic Kerr' nonlinearity, as was assumed in the original proposal [101,102,103], the equation of motion for the deviation of the refractive index from its value in thermal equilibrium is

$$\frac{d}{dt}n = -\gamma n + D\Delta_\perp n + P, \tag{12}$$

where γ is a relaxation rate, $\Delta_\perp$ is the transverse part of the Laplacian modeling some nonlocal coupling within the medium, D is the corresponding 'diffusion' constant, P denotes the pump rate being proportional to the sum of the intensities of the forward (E_f) and the backward (E_b) field, whose amplitudes are suitably scaled. The transmitted field is given by

$$E_t = E_{\text{in}} \exp\left(-i\chi k_0 L/2\right), \tag{13}$$

where L is the length of nonlinear medium and the dielectric susceptibility for the model Kerr medium assumed here is $\chi = 2n$. The backward field is calculated from the transmitted one by taking into account its propagation in free space and the reflection from the mirror with reflectivity R:

$$E_b = \sqrt{R} e^{-id\Delta_\perp/k_0} E_t, \tag{14}$$

Note that E_t and hence E_b and P depend on n. Thus (12) is a nonlinear, nonlocal partial differential equation.

The refractive index change n could have many different physical origins. It might be due to highly off-resonant excitation in an atomic medium, due to a change of a carrier concentration in a semiconductor (at weak excitation) or due to a field-induced reorientation of the director orientation in a liquid crystal. Indeed, soon there were plenty of realizations of the proposed scheme using a variety of different nonlinear media. We refer to review articles and the references given therein for an overview [3, 6]. Typically, the first structures bifurcating at threshold are hexagons [102, 103, 3, 6] and in at least two cases it was shown explicitly shown that they may bifurcate subcritically from the

homogeneous state [119,120]. Hence, already one of the prerequisites identified above for the formation of solitons is fulfilled.

We will now concentrate on the case where the nonlinear medium is sodium vapor driven in the vicinity of the D_1-line. The use of an atomic vapor has the advantage of combining a rather high all-optical nonlinearity with a good optical quality and the possibility of a well established description of the light-matter interaction in terms of the semiclassical density matrix formalism. Very interesting experiments on localized states and solitons have also been performed in the so-called liquid-crystal light-valves [121, 104, 105, 108, 112, 109, 113, 115, 116].

5.2 Experimental setup

The experimental setup (Fig. 13) consists of a cell containing sodium vapor in a nitrogen atmosphere and a plane feedback mirror at some distance d behind the medium. The cell is heated over a length of 15 mm, while the ends are cooled. The cell temperature is varied in the range around 320°C, yielding a particle density of 10^{19} m^{-3} to 10^{20} m^{-3}. The buffer gas (pressure typically 200 - 300 hPa) reduces the diffusion, provides a homogeneous linewidth masking the Doppler effect and the hyperfine splitting of the ground state and it quenches the excited state in order to prevent diffusion of radiation. The cell is placed in a magnetic field **B** which has a non-vanishing longitudinal (z-axis) and transverse component (x-axis) with respect to the direction of the laser beam.

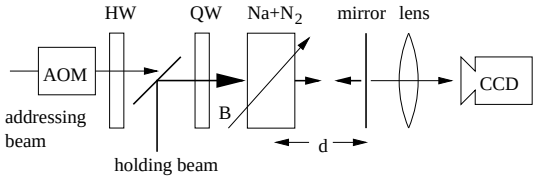

Fig. 13. Scheme of the experimental setup. AOM: acousto-optic modulator, QW: quarter-wave plate, $Na+N_2$: sodium-cell, CCD: charge-coupled device camera.

The output beam of a cw dye laser, which is stabilized in frequency and intensity, is carefully spatially filtered by transmitting it through a single mode fiber. After the fiber, the beam is collimated (w_0 = 1.5 mm, radius at $1/e^2$–point of intensity) and injected into the sodium cell. We will refer to this beam as the 'holding' or 'background' beam. It is circularly polarized and the detuning Δ of its frequency with respect to the resonance of the Na–D_1 is chosen to be about 10 GHz to the blue side. Under these conditions the nonlinearity has both a dispersive and an absorptive contribution.

A small amount of light is split off the main beam and serves as an 'addressing beam' which 'ignites' the solitons. It can be gated by an acousto-optical

modulator (AOM). The radius ($1/e^2$) of the addressing beam is 0.17 mm. Its polarization state and frequency is discussed in more detail below. The power in the background beam within the sodium vapor is in the order of 100 mW and in the address beam about 1 mW.

The feedback mirror has a reflectivity of $90 \ldots 99\%$. The transmitted part of the light passes a lens which can focus more or less arbitrary planes of the beam path onto the image plane of a CCD camera. If not stated otherwise the imaged plane is at a distance $2d$ behind the sodium cell, i.e. the recorded intensity distribution corresponds to the reflected and re-entrant field E_b.

5.3 Optical pumping nonlinearity in alkali metal vapors

For the conditions of the experiment, the optical nonlinearity on the D_1–line can be described in the framework of the homogeneously broadened J=1/2→J'=1/2 transition depicted in Fig. 14a. Angular selection rules allow the creation of a population difference between the two Zeeman sublevels of the ground state. If we assume e.g. excitation with σ_+–light, then only the $m_J = -1/2$–substate of the ground state absorbs, but both are repopulated by the relaxation processes (spontaneous emission and quenching of the excited state by collisions with nitrogen molecules). The relaxation is even isotropic for the conditions of the experiment since the populations in the sublevels of the excited state are rapidly equalized by the collisions with the buffer gas. This process is referred to as *optical pumping* [122] and leads to a rather efficient optical nonlinearity.

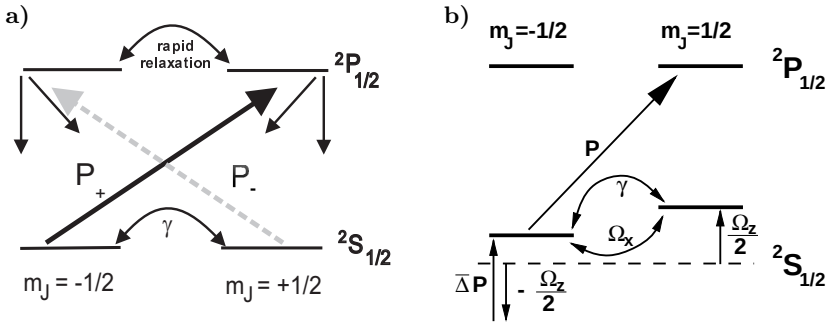

Fig. 14. a) Kastler diagram of a J=1/2→J=1/2 transition driven by σ_+-light (solid black arrows) and/or σ_--light (dashed grey arrows). b) Modified Kastler diagram for blue detuned excitation with σ_+–light in the presence of an oblique magnetic field. For simplicity, the splitting of the excited state is not shown. The dashed line indicates the position of the ground state of the bare atom.

The existence of a population difference between magnetic sublevels implies the existence of a macroscopic magnetic moment of the sample. This will

precess in an external magnetic field. If the direction of propagation of the laser beam is used as the axis of quantization (z-axis), then the presence of a transverse component B_x of the magnetic field causes changes in the z-component of the magnetic moment, i.e. 'spin-flips' between the Zeeman sublevels occur (Fig. 14b). The mechanism is most effective if the longitudinal component B_z vanishes. In a quantum mechanical description the light-induced level-shift has to be taken into account (Fig. 14b). It acts like an extra contribution to the z-component of the magnetic field and is proportional to the intensity times the detuning of the laser with respect to the atomic resonance.

In a formal description it is convenient to introduce the Bloch vector $\mathbf{m} = (\mathbf{u}, \mathbf{v}, \mathbf{w})$ which is proportional to the ground–state orientation of the sodium vapor [123]. Its equation of motion is given by [124]:

$$\partial_t \mathbf{m} = -(\gamma - D\Delta_\perp)\mathbf{m} + \hat{\mathbf{e}}_z P - P\mathbf{m} - \mathbf{m} \times \mathbf{\Omega}. \tag{15}$$

The first three terms are identical to the ones we know already from the Kerr case, Eq. (12). Here, they are interpreted as collision-induced relaxation, thermal motion of the sodium atoms in the buffer gas atmosphere, and optical pumping. The next term describes the saturation of the optical nonlinearity and would be also present in models for two-level atoms and semiconductors. The components of the vector $\mathbf{\Omega} = (\Omega_x, 0, \Omega_z - \bar{\Delta}P)$ are the Larmor frequencies produced by B_x and B_z, respectively, with the latter being modified by a light-shift term [123]. $\bar{\Delta}$ is the detuning between the incident field and the atomic transition, normalized to the relaxation constant Γ_2 of the polarization of the medium. The complex susceptibility of the vapor depends on the longitudinal component w of the orientation through [123]

$$\chi = -\frac{N|\mu|^2}{2\hbar\epsilon_0\Gamma_2}\frac{\bar{\Delta}+i}{\bar{\Delta}^2+1}(1-w) \equiv \chi_{lin}(1-w), \tag{16}$$

where N is the sodium particle density. The equations for the transmitted and re-entrant field distributions were given in (13) and (14).

The homogeneous solution for the steady state of w is given by

$$w_0 = \frac{P_0}{\gamma + P_0} \quad \frac{(\Omega_z - \bar{\Delta}P_0)^2 + (\gamma + P_0)^2}{(\Omega_z - \bar{\Delta}P_0)^2 + (\gamma + P_0)^2 + \Omega_x^2}, \tag{17}$$

where $P_0 = P_{\rm in}(1 + R|\exp(-ik_0 l\chi_{lin}(1-w_0)/2)|^2)$. Equation (17) has the interesting property that it has a a resonance–like dependence on the term $\Omega_z - \bar{\Delta}P_0$, i.e. there can be a pronounced minimum of the orientation for a well–defined finite light intensity (see Fig. 15). This is a manifestation of a 'light-shift induced level-crossing' produced by the combined action of Zeeman splitting and light-shift (Fig. 14b, [124,6]). In the presence of optical feedback the corresponding characteristic curve describing the homogeneous solution of the orientation can become very steep (see Fig. 15) or even bistable [124,111]. There is some analogy between the z-component of the magnetic field in the feedback system and the detuning parameter in a cavity, although we warn that one should not take this analogy too seriously: Ω_z as well as θ

determine where (and whether) on the pump axis OB occurs. In addition, a nonlinear resonance might occur in both cases, if Ω_z or θ are ramped at constant pumping. However, there is no continuous dependence of the selected spatial scale on Ω_z as it is on θ in the cavity case.

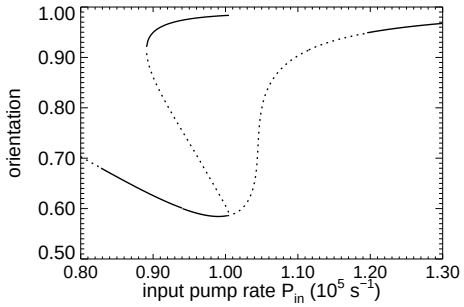

Fig. 15. Solutions and their stability properties, both obtained from semi-analytical calculations. The sigmoid curve extending over the whole range of pump parameter depicts the homogeneous, steady–state solution (orientation versus input pump rate). The dashed parts are unstable against periodic perturbations at a finite transverse wave number. The additional curve in the central range of pump parameter depicts the maximum orientation of a branch of feedback solitons (FS) bifurcating subcritically from the homogeneous solution at $P_0 = 100500\ \mathrm{s}^{-1}$. Again the dashed part is unstable. Parameters: $\Omega_x = 1.2 \times 10^5$ rad/s, $\Omega_z = 9.0 \times 10^5$ rad/s, $\Delta = 10.0$ GHz, $d = 70$ mm, $N = 3.0 \cdot 10^{13}\ \mathrm{cm}^{-3}$, $D = 237\ \mathrm{mm}^2/\mathrm{s}$, $\gamma = 1.5\,\mathrm{s}^{-1}$, $\Gamma_2/(2\pi) = 1.6$ GHz, $L = 15$ mm, $R = 0.915$ (from [114]).

In the following, we will investigate the behavior of the system in the vicinity of the minimum of the characteristic curve in a situation in which the homogeneous characteristic is very steep, i.e. close to being bistable ('nascent optical bistability', Fig. 15).

6 Basic results

6.1 Switch-on and -off procedure

Fig. 16 illustrates the process of igniting and erasing a FS. The system is prepared in an 'unstructured' state by slowly increasing the power of the background beam from low values until the working point close to the minimum of the transmission curve is reached (leftmost image in Fig. 16). Then the polarization of the addressing beam is adjusted by means of a half–wave plate such that it is the same as that of the background beam after recombination. This means that the two beams are circularly polarized with the same helicity after the quarter–wave plate. When the addressing beam is then switched on,

a bright spot emerges at the position of the addressing beam (second image from the left). This spot remains stable after the addressing beam is switched off (central image of Fig. 16). The shape of the central lobe deviates from a Gaussian and it is surrounded by weak dark and bright diffraction fringes (see also Figs. 19, 18), i.e. it deviates from the Gaussian profile of the addressing beam. This indicates that this bright peak is an attractor of the dynamics.

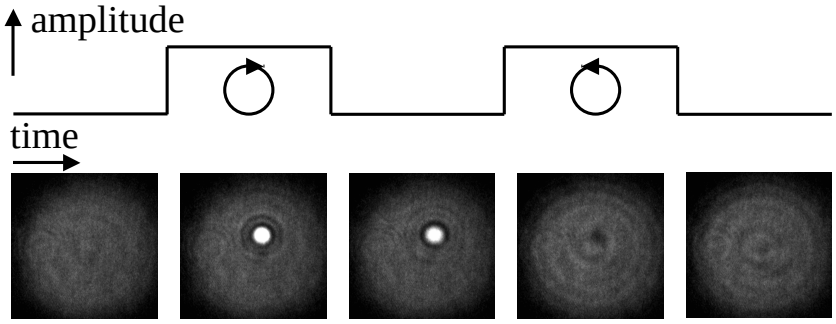

Fig. 16. Ignition and erasure of a localized state with the addressing beam. The upper part of the figure shows schematically the amplitude of the addressing beam, the lower row the near field intensity distribution of the beam reentering the medium. Parameter: $d = 70$ mm, $\Delta = 8.2$ GHz, $B_\perp = 2.59\,\mu$T, $B_z = 19.2\,\mu$T, cell temperature 312.3°C, $p_{N_2} = 197$ hPa, $P_{in} = 100$ mW. The images are plotted in a linear grey–level scale with white denoting high intensity. The absolute scale was adjusted such that the background beam is always clearly visible; therefore the center of the FS is overexposed. The frame size is 2.6 mm×2.6 mm (from [111]).

Now the polarization of the addressing beam is rotated by 90° by turning the half–wave plate; therefore the background beam and the addressing beam are still circularly polarized in the medium but with *opposite helicity*. If the addressing beam is switched on again at the position of the peak, a dark hole appears (second image from the right in Fig. 16). The hole disappears after the addressing beam is switched off again. Thus the bright peak is erased and the homogeneous state is reached again.

This procedure can be repeated over and over again. This observation proves that there is bistability between a state with one bright peak on an unstructured background and the unstructured background alone. This is the expected behavior for a FS or a CS.

The remaining question needed to be answered is why we can utilize 'polarization' of the opposite helicity to erase a FS, whereas we stated in the first sections that an addressing beam of opposite phase should be used. The reason becomes immediately clear by looking at Fig. 14a. Circular polarization components of opposite helicity pump antagonistically. Hence, it is possible to mimic destructive interference by using the opposite polarization component (see, e.g., Eq. (7) of [111] for the complete equations). This has the addi-

tional advantage that there is no need for interferometric stability between the beam pathes of the holding and the addressing beam, since light of opposite polarization does not interfere. Indeed, the frequency of the addressing beam was shifted from the frequency of the holding beam by 140 MHz due to the presence of the AOM. Hence, even the switch-on is created by an incoherent superposition of the holding and the addressing beam again eliminating the need for interferometric path length stability. We remark that, of course, switching of FS is also possible by using constructive and destructive interference of coherent beams of the same circular polarization, however this scheme is considerably less robust.

These observation obviously motivate considerations on whether polarization degrees of freedom might be utilized for phase–insensitive control of CS in semiconductor microcavities. We remark that the phase–insensitive control of all-optical flip–flops based on small–area semiconductor amplifiers was achieved by injecting beams of very different wavelength (several tens of nm) which perturb incoherently the carrier concentration [125]. For the case of CS, interesting studies exist using beams of orthogonal linear polarization [85]. However, the mechanisms of incoherent switching are unclear and a complete control of ignition and erasure was not achieved, yet.

In general, the FS are not stable at the positions at which they are ignited, but they start to drift after the addressing beam is switched off. This is due to a drift motion of the FS in intensity and phase gradients of the light field as discussed in the preceding sections for CS. In a rotationally symmetric holding beam, the FS will be trapped either in beam center or on a ring with a certain distance from the center, since these are the points equivalent by symmetry. For the present situation, the amplitude gradients pull the FS towards the center, whereas the phase gradients push them out. As a result, there is a stable equilibrium at a finite distance from beam center. This is very apparent where more than one FS exist on the beam (Fig. 17). This issue is discussed in more detail in [114, 110].

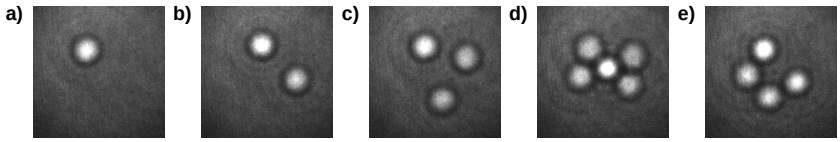

Fig. 17. Stable clusters of localized structures. The images are overexposed in order to emphasize the diffraction fringes surrounding each localized structure. Parameters: $B_\perp = 0.78$ μT, $B_\parallel = 14.40$ μT, $\Delta = 18.6$ GHz, $d = 70$ mm, $p = 310$ mbar, $T = 315°$ C. Power: a) 131 mW, b) 133 mW, c) 133 mW, d) 135 mW and e) 138 mW. The transverse size of the images is 2.6 mm (from [107]).

6.2 Existence of FS: theory

Fig. 15 shows the calculated homogeneous solution for the orientation versus the input pump rate for a typical situation in which the experiments with FS have been carried out. After the minimum, the homogeneous characteristic has a sigmoid form, which corresponds to the situation of 'nascent optical bistability' for which many semi-analytical studies of CS were done [64, 74]. The sections of the homogeneous solution that are drawn dashed are linearly unstable against periodic perturbations at a finite wave number, i.e. there is a pattern forming modulational instability (MI) [126]. We will investigate this in more detail below (see Sect. 7.2).

For a calculation of the soliton branches a method similar to the one discussed above for CS is utilized, i.e. we will analyze in the following the system which is obtained from Eq. (15) by setting the time derivative to zero. In order to simplify the calculations, radial symmetry is assumed. Then, the stationary states are found by discretizing the differential equation in space and searching for solutions of the resulting large set of coupled equations with a Newton method. The fact that in the feedback problem, Eq. (14), the Laplacian operator appears in an exponential whereas it is only first order in the cavity case, Eq. (1), constitutes a technical difficulty which is solved by evaluating the derivatives by a Hankel transform method in Fourier space [127].

The calculations show that a branch of FS emerges from the homogeneous state at the point where the homogeneous state becomes modulationally unstable near the minimum of the characteristic ($P_{\mathrm{in}} = 1.005 \cdot 10^5 \mathrm{s}^{-1}$, Fig. 15). The branch bifurcates backwards, turns around at $P_{\mathrm{in}} = 0.891 \cdot 10^5 \mathrm{s}^{-1}$ and terminates again at a point which coincides with the MI point with a relative deviation of less than 10^{-3}. Here, the FS becomes unstable against the formation of spatially extended patterns. With the present accuracy of the program code, it is not sure, whether the two points coincide or not.

The upper part of the branch is stable, the lower unstable, i.e. the bifurcation to the FS is subcritical. Between $P_{\mathrm{in}} = 0.891 \cdot 10^5 \mathrm{s}^{-1}$ and $P_{\mathrm{in}} = 1.005 \cdot 10^5 \mathrm{s}^{-1}$ FS coexist with the homogeneous solution. At the limit point $P_{\mathrm{in}} = 0.891 \cdot 10^5 \mathrm{s}^{-1}$ they disappear via a saddle–node bifurcation. The similarity to the bifurcation behavior of CS depicted in Fig. 3 is obvious.

Fig. 18a shows the calculated profile of a FS on a plane–wave background. It consists of a high–amplitude central peak which is surrounded by oscillating tails. This matches the experimental observation. For $x \to \pm\infty$ it approaches the homogeneous solution. Numerical simulations of the full two–dimensional equations show that it can exist anywhere in the transverse plane, if a plane wave input beam and periodic boundary conditions are used. Furthermore several FS can exist at the same time at different positions of the transverse plane. These properties are completely identical to those of CS (cf. Fig. 5b for the profile of a corresponding CS). In the experimental realization there is – as already discussed – no complete arbitrariness of positioning since the

symmetry of the system is reduced due to the radial gradients induced by the Gaussian input beam.

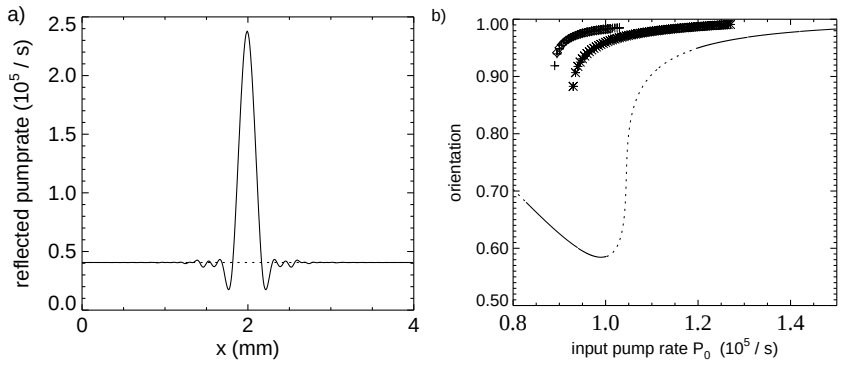

Fig. 18. a) Transverse cut through the center of a calculated FS for a plane–wave background beam for $P_{\rm in} = 0.96 \cdot 10^5 {\rm s}^{-1}$ (other parameters as in Fig 15). The graph shows the pump rate of the reflected field versus one transverse coordinate. b) Bifurcation diagram for spatially extended periodic patterns. Shown is the maximum orientation versus the pump rate. The lower curve corresponds to the homogeneous solution. It is unstable in the dotted part. The wavenumbers of the patterns are: Double crosses (lower right curve) 17.1 $\rm mm^{-1}$, crosses 10.2 $\rm mm^{-1}$, rhombs 7.9 $\rm mm^{-1}$ (from [114]).

Since the bifurcation to FS is subcritical one can create a FS by a large–amplitude perturbation (sometimes called 'hard' perturbation) in the bistable region before the bifurcation point. This is the region in which the experiment described above was performed. The unstable branch will be very important in the turn-on experiments discussed below since it defines the separatrix in phase space.

6.3 Mechanism of stabilization

As mentioned in the description of the experimental setup, the plane imaged onto the camera can be varied. Thus the change of the intensity distribution in the light field during its propagation in the free space between the nonlinear medium and the feedback mirror and also behind the mirror can be monitored. The latter corresponds to the intensity distribution in the backward beam, of course. Corresponding results are shown in Fig. 19a. At the position of a FS, there is an intensity peak at the exit window of the cell. During the propagation of the beam, however, the central intensity increases strongly and simultaneously the width of the peak decreases. This behavior is possible if the main effect of the FS is a phase modulation that creates locally a concave deformation of the wavefront which makes the beam locally

converge to a focus. The central intensity reaches a peak and then declines, but when the beam reenters the medium after being reflected it still has a very pronounced intensity peak, surrounded by wiggles which obviously correspond to diffraction fringes. The behavior is reproduced well in simulations (Fig. 5a of [110]). These also confirm that there is a strong local curvature of the phase surface introduced by the FS (Fig. 19b).

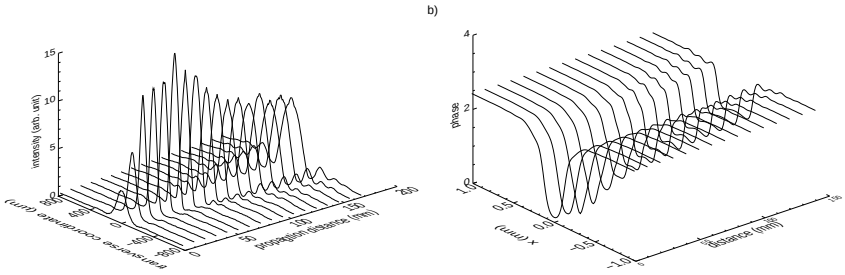

Fig. 19. a) Observed profiles of the intensity distribution produced by a FS during propagation from the sodium cell to the mirror and back. Parameters: $B_x = 4.17\ \mu$T, $B_z = 8.23\ \mu$T, $\Delta = 13.5$ GHz, $d = 80$ mm, $P_{las} = 107$ mW, $T = 340.0°C$, $p_{N_2} = 216$ hPa (from [107]). b) Numerically calculated phase distribution produced by a FS during the propagation between the sodium cell and the mirror and back. Parameters: $\Omega_x = 1.2{\cdot}10^5$ rad/s, $\Omega_z = 9.0{\cdot}10^5$ rad/s, $\Delta = 10.0$ GHz, $\gamma = 1.5\ \mathrm{s}^{-1}$, $D = 237\ \mathrm{mm}^2\mathrm{s}^{-1}$, $\Gamma_2 = 1.0{\cdot}10^{10}\ \mathrm{s}^{-1}$, $N = 0.3{\cdot}10^{20}\ \mathrm{m}^{-3}$, $d = 70$ mm, $P_{\mathrm{in}} = 96000\ \mathrm{s}^{-1}$ (from [110]).

It can be concluded that the mechanism of the formation of the FS is the following: the address beam locally introduces a distribution of the orientation which acts like a focusing lens. This lens introduces a phase encoding which makes the diameter of the local field distribution shrink until the focus is reached. The process works best if there is a strong dependence of the orientation on the intensity, as in the case of nascent OB. Indeed in the corresponding intensity range the medium is self-focussing, while it is self-defocusing at the intensity level of the background beam which corresponds to the descending slope of the plot (Fig. 15). It will be of importance in Sect. 7 that strong diffraction fringes occur in the process.

We mention that the stabilization of localized states by self-induced lensing was suggested first, to our knowledge, in [128,49] for plano-planar cavities with a liquid-crystal nonlinearity. It can be shown that even in a simple lensing model the scaling of the size of a FS with wavelength and mirror distance is the same as the scaling for the pitch of a pattern due to the Talbot effect, Eq. (11), [129]. We commented on the generality of this scaling behavior already before in the CS case (see also [49]).

This interpretation of a FS seems to correspond best to the 'soliton-in-a-box'-picture of CS, i.e. in the 'half-cavity box' formed by the medium and the

mirror a self-consistent localized state forms due to the interplay of nonlinear refraction (lensing) and diffraction. We mention that the analogy can be made even closer by regarding the medium as an 'active mirror' [130,131], although to our knowledge this idea was not worked out for localized states. However, we will see that the 'part-of-a-pattern'-interpretation can also be applied in the FS case.

7 Interaction behavior

7.1 Interaction between two solitons

An analysis of images containing several FS (e.g., Fig. 17) suggests that certain distances between single FS are preferred by the system. For a detailed analysis we recorded a large number of images for fixed experimental parameters at a constant time interval of 200 ms. Within this time, typically spontaneous transitions between different configurations of FS occur. The observed configurations varied in the number of constituents (from 1 to 3) and in the position of the FS on the preferred ring around the beam center. These different configurations are interpreted as manifestations of the high degeneracy of the situation because of multistability due to symmetry and due to the coexistence of several states. Random transitions between these states occur due to noise. For the histogram of distances displayed in Fig. 20g the subset of images containing only two FS has been considered.

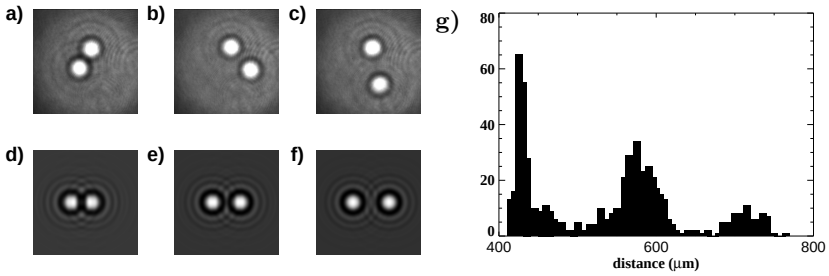

Fig. 20. Stable configurations of two localized structures. a) – c): Experiment (overexposed in order to visualize the diffraction fringes), parameters: $B_\perp = 2.36\ \mu$T, $B_\parallel = 10.98\ \mu$T, $\Delta = 13.9$ GHz, $d = 63$ mm, $p = 200$ mbar, $T = 316°$C. d) – f): Numerical simulation, parameters $B_\perp = 3.94\ \mu$T, $B_\parallel = 15.72\ \mu$T, $\Delta = 9.5$ GHz, $d = 63$ mm, sodium particle density $N = 0.3 \cdot 10^{14}$ mm^{-3}. The transverse size of the images is 2020 μm. g) Histogram of distances between two localized structures; 669 images are evaluated (from [107]).

A preference for three discrete values of the distance is clearly visible from Fig. 20. By weighted averaging over the three humps we find the values 445

μm, 573 μm and 717 μm. Fig. 20 a) – c) shows typical examples of these configurations. The peaks for larger distances between two FS are broader than the first peak; the reason for this result is probably that the configurations with a larger distance are more sensitive to noise or parameter fluctuations. The images of the bound states depicted in Fig. 20a) and d) are the analogue to the cavity case depicted in Fig. 5f).

For studying the interaction behavior calculations are carried out under the assumption of a plane wave background beam. In this way the drift of the FS in a gradient of the background is eliminated. It turns out that – depending on the initial distance between two FS – they either attract or repel each other until a stable distance is achieved. The resulting histograms are much sharper than the experimental one proving that the stable configurations belonging to bound states of FS are indeed discrete. Fig. 20 d) – f) show the configurations for the three smallest stable distances between two FS. The corresponding distances are 393 μm, 533 μm and 691 μm, i.e. they show a rather close correspondence to the experiment. We find even larger distances than these three, but they are rather unstable with respect to noise.

As explained in the sections on CS, stationary solitons have a neutral mode related to the translational symmetry. Consider now the perturbation of a soliton with respect to another soliton. The oscillations of the phase and amplitude of the soliton field as it dies away into the background field will provide a perturbation to the other soliton. This perturbation induces a drift motion with some velocity. We can expect to find equilibrium positions where the relative velocity is zero, and that these define stable or unstable bound states of two solitons. Because the solitons are surrounded by several diffraction fringes, a large number of equilibrium positions can be expected between two solitons. Only the smallest distances, however, are observed in the limited beam. Furthermore we observe numerically that the stability of a bound state of FS against perturbations decreases with increasing distance, which is consistent with the fact that the amplitude of the fringes decreases. The pitch of the diffraction fringes and the corresponding distances between the FS depend on the mirror distance d with roughly the same scaling as for extended patterns (Eqs. (11)). They can be also changed to some extent by introducing a Fourier filter in the feedback loop [127, 112].

Obviously, it is worthwhile to strive for analytical insight into the FS interaction, especially on the establishment of a concrete relationship between the pitch of the diffraction fringes and the mutual distances. This is however quite difficult to perform in the present system, since intensity fringes do not interact directly, but the interaction is mediated rather by the spatial profiles in the three different components of the Bloch vector induced by the intensity profile. The spatial profile of these components can be quite different, e.g. u has a hole at the positions of a FS. In addition, strength and position of the ripples in the Bloch vector components depend on diffusion. Hence the situation is more complicated than in a Kerr medium (with negligible or only small diffusion), in which there is a 1:1 correspondence between intensity and

the induced refractive index. Nevertheless, our observations are backed up, complemented and extended by recent nice experiments on FS interaction in liquid-crystal light-valves with a Kerr-like nonlinearity [112, 115]. This establishes a rather universal behavior of FS. A corresponding interaction behavior is also found for CS [75,84,81,21,54,71] for nonlinearities based on a intensity dependence of the refractive index as well as on saturable absorption. For CS, semi-analytical studies were performed revealing quantitatively the interaction potential [21, 54, 71, 132]. Actually, the universality applies not only for FS and CS but even for dissipative solitons in non-optical systems [99] (and Refs. in [107]). However, in some sense this is not too surprising since the qualitative aspects of solitons with oscillatory tails should be fixed by symmetry considerations.

An analysis of the clusters with more than two constituents in Fig. 17 reveals that most of the distances observed between the constituents appear already in the bound states of two single FS for identical parameters; the deviations are characteristic for the type of cluster. It should be kept in mind, however, that in the experiment the shape of the clusters is not only a result of the interaction of FS with each other, but also of the interaction of the FS with the inhomogeneous holding beam – favoring positions on ring segments.

7.2 Connection between solitons and extended patterns

The results of a linear stability analysis of the homogeneous state reported in Fig. 15 show that the FS branch arises from a point in which the homogeneous solution becomes unstable versus spatially periodic perturbations, i.e. pattern formation. Indeed, it was also established experimentally, that the existence region of FS is at the boundary of the existence region of spatially extended patterns (Fig. 4 of [111]).

Fig. 18b shows three branches of perfect periodic hexagonal pattern existing in the parameter regime discussed in Fig 15. These patterns differ by their length scale. The branches of two of these (with a wavenumber of 10.2 mm^{-1} and 7.9 mm^{-1}) are very similar to each other and to the FS branch depicted in Fig 15 except for the fact that the pattern branches extend in the MI region. The third branch has a wave number of 17.1 mm^{-1} and has a different amplitude and existence range. Interestingly, the next-neighbor distance between two spots of the hexagonal patterns corresponds nearly exactly to the distance between the FS in bound states of two FS for these parameters. This holds for all three patterns (distances in bound states: 434 μm, 720 μm, 937 μm; next neighbor distances in patterns: 424 μm, 711 μm, 918 μm [127]) This suggests a 'FS = part of a pattern' interpretation like in the case of CS discussed above. Using suitable initial conditions also a great variety of clusters and of patches of hexagonal patterns surrounded by voids ('localized patterns') can be found (Fig. 21a-c). It is also possible to create patterns in which single or multiple constituents are missing (Fig. 21d, e), [133]). Corresponding states were discussed above for CS (see also [64, 71, 56, 87, 73]).

We warn that the perfect patterns mentioned above as well as the closely packed localized patterns form only, if they are seeded. Otherwise spatially irregular states with clusters of FS and voids in between them emerge, if simulations are started from noisy initial conditions above or below the MI point (Fig. 19 of [114]). These show a great similarity to the 'cracking hexagons' obtained for CS [55].

The results on bound states of FS or CS indicate the intriguing possibility to build up nearly arbitrary states from (weakly) interacting FS or CS which serve as 'quasi-particles'. The perfect patterns might be also interpreted as being due to weakly interacting FS (see the discussion above for CS, see also [84,87]). The interpretation of the pattern with a wavenumber of 17.1 mm^{-1} is not quite clear, since there the constituents differ significantly from the shape of a single FS.

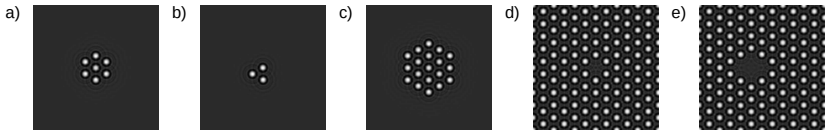

Fig. 21. Localized patterns with the same pitch as the extended pattern with 10.2 mm^{-1} in Fig. 18b). $P_0 = 90000\ \mathrm{s}^{-1}$ (from [114]).

Finally, we note that obviously bistability between plane wave states is not a prerequisite for FS (see Fig. 15). We obtained this result for CS before (see also [57, 132]). What is needed is bistability between a plane wave state and a spatially extended pattern. Nevertheless, we find numerically that FS only exist, if the slope of the homogeneous characteristic is 'sufficiently high', i.e. if one is 'sufficiently close' to nascent OB (see Fig. 6 of [114]). We are not aware of a rigorous analysis of the situation, but it seems to be reasonable that large-amplitude structures like FS or CS are somehow favored by the existence of the second high-amplitude branch. For patterns, modifications of the standard bifurcation in the vicinity of bistability between plane wave states is known [134, 133, 132].

8 Applications

Arrays of cavity solitons may have applications in parallel information processing [135]. They can be created at any location by a suitable address pulse, and are non-diffracting and dynamically stable, all of which makes them suitable 'bits' for image or data capture, storage and processing. This has been demonstrated numerically in [65] and confirmed in the prototype experiments discussed above and in [104, 105, 85, 88, 86]. Cavity and feedback solitons also

offer functionalities which are beyond any micro-structured material array, whether optical or electronic. In particular, we have seen that they can be optically manipulated, e.g. by imposing a spatial phase profile on the driving field [65, 77, 54]. Processing schemes which take advantage of their unique properties may avert the unequal competition with silicon which has plagued other all-optical processing schemes.

Any perturbation to the pump field which has a finite gradient at the soliton location will couple to the 'neutral mode' identified above, and cause the soliton to move. This has implications for the response of CS and FS to noise and to any stray gradients, and also for interaction between them, as is illustrated by the experimental results on FS discussed above. This coupling can also be used positively, to *control* the motion and location of the solitons through the spatial phase profile of the pump field. One can think of the solitons in a 'landscape' determined by the phase of the holding (control) field, a landscape in which they move in response to phase gradients. Thus a simple memory array [65] consists of a regular landscape of 'hills' and 'valleys', with the solitons attracted to the peaks. Unlike one formed from machined pixels, however, this landscape is reconfigurable by changing the phase profile of the control field. This allows these 'soliton bits' to be manipulated, by either global or local reconfigurations of the control field. This plasticity opens up possibilities for novel processing functions and applications [135]. In the following, we will discuss two prototype experiments which give proofs of principle of these ideas for FS in sodium vapor.

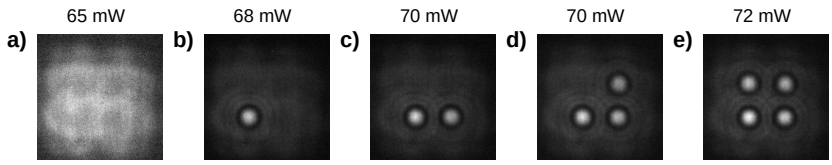

Fig. 22. Pinning of FS on positions that are prescribed by modulations in the background light field. Parameters: $B_\perp = 2.38\,\mu$T, $B_z = 7.55\,\mu$T, $\Delta = 12.0$ GHz, $d = 70$ mm, $T = 303.0°$C (from [110]).

First, we show how 'FS bits' can be pinned to a fixed position in the transverse plane by spatial modulations of the holding beam. For the experiment shown in Fig. 22 this proposal has been realized in a very simple manner by introducing a quadratic aperture into the input beam and thus inducing a quadratic diffraction pattern. The small amplitude modulations appearing in the background beam can be seen in Fig. 22 (a). In addition, there will be phase modulation. We are able to create a 2×2–Array of FS: When the input power is increased, the FS pop up spontaneously on the four positions prescribed by the diffraction pattern. Probably because of small misalignments in the experimental setup we did not succeed in producing bistability between

the states with and without FS on all four positions simultaneously. In addition to the pinning of FS, this feature would be necessary for an optical memory.

Another possible application that uses FS as optical bits is demonstrated in Fig. 23. Here the feedback mirror has been slightly tilted in order to initiate a drift motion of the FS. In the experiment shown in Fig. 23 the direction of the drift motion is upwards. For $t = 0\,\mu$s there is one FS in the upper part of the background beam and a second FS is being created with the addressing beam in the lower part. Therefore in the following the system is in a state where two storage positions are occupied with a FS. After $64\,\mu$s the upper FS has disappeared, at $t = 80\,\mu$s a new FS has been created in the lower part. An empty storage location can be created simply by omitting the addressing beam in one cycle.

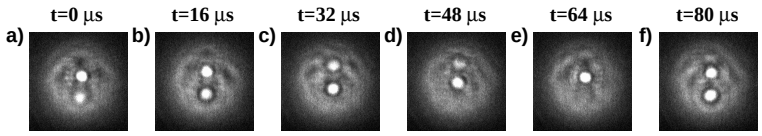

Fig. 23. Optical buffer register. The FS are drifting upwards since the feedback mirror is tilted. New FS are created in the lower part of the image by the addressing beam with a frequency of 14 kHz. Parameters: $B_\perp = 0\,\mu$T, $B_z = 14.41\,\mu$T, $P_0 = 115$ mW,$\Delta = 11.9$ GHz, $d = 70$ mm, $T = 329.5°$C (from [110]).

Such an all–optical buffer register could be used in optical telecommunications for the translation of serial data into parallel data, or could serve as a buffer for the temporary storage of data [136], which is considered to be a key-element of future all-optical communication and processing networks. Since the drift velocity of the FS depends on the tilt angle of the feedback mirror, the delay of the buffer register can be adjusted easily. In the situation considered here, the total number of FS is rather limited due to the small beam radius. However, in principle much larger systems are accessible, if the material questions are solved. Fig. 24 shows a simulation of an optical buffer memory using drifting CS (saturable absorber model) for a homogeneous, but phase-tilted, input beam. Note that such schemes depend on the non-diffracting property of a CS or FS: an ordinary beam created by a bit-pulse would diffract as it drifted, and the information would be lost.

For applications, it is very important to determine the response and switching times of FS and CS. Hence, we next discuss the transient evolution of the ignition process of a FS. The power of the background beam is adjusted such that the system is in the unstructured branch within the bistable region. The switching process is observed with a fast photodetector placed in the near field image plane at the location of the addressing beam.

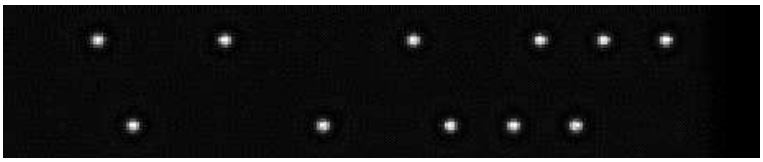

Fig. 24. Two frames from a soliton buffer memory simulation in the saturable-absorber cavity 3. CS are written at the left by "1" pulses of an optical bit-stream, and drift rightwards on a uniform phase gradient (from [135]).

The ignition pulse used in the experiment has a width of 1.7 μs (dashed curve in Fig. 25a). Obviously the detector monitoring the transmitted light has to show a corresponding signal during the time interval in which the addressing pulse is present (solid curve in Fig. 25a). Afterwards the transmission drops again to nearly the initial value, but the switching process has been started. In the example shown it takes 25.4 μs (using a 50%–criterion) until the FS is finally switched up. The success of the ignition process depends on the amplitude I_a as well as on the duration of τ_a of the addressing pulse. For zero–dimensional bistable systems it was found that for switching pulses that are short compared to the relaxation of the medium, only the pulse area, i.e. the product $F = I_a \cdot \tau_a$ in the case of a rectangular pulse, is the decisive factor [137, 138, 139, 140]. Although we did not perform the systematic studies necessary to establish a pulse area law strictly, it will be seen in the following that our experimental results for various amplitudes and widths are in accordance with such a law.

Fig. 25b shows the distribution of switching times versus a control parameter ϵ, which is related by $\epsilon = (F_a - F_c)/F_c$ to the pulse area F_a and the critical pulse area F_c. The switching time increases logarithmically, if ϵ is decreased. The increase of the switching time observed in the experiment is called *noncritical slowing down* and has been established for zero–dimensional bistable systems [138, 139, 140]. It may be useful to call the interpretation of the phenomenon to mind: the action of the short addressing pulse is integrated over its duration and puts the system in phase space beyond the separatrix. ϵ parametrizes the distance to the separatrix. After the addressing pulse relaxational dynamics towards the stable fixed point takes place. If one starts close to the separatrix (unstable fixed point) the dynamics is governed by the exponential growth of deviations from this fixed point, which explains the observed logarithmic dependence of the switching time on the (excess) pulse area of the addressing beam.

Non-critical slowing down was discussed before numerically as well as analytically for CS [43, 54, 56] and was experimentally observed for LS in a liquid crystal light valve [104, 105] with switching times in the regions of some hundreds of milliseconds. Obviously, these switching times as well as the ones obtained here, are not very attractive for applications. However, the switching times scale somehow with the relevant relaxation rates, though, of course the

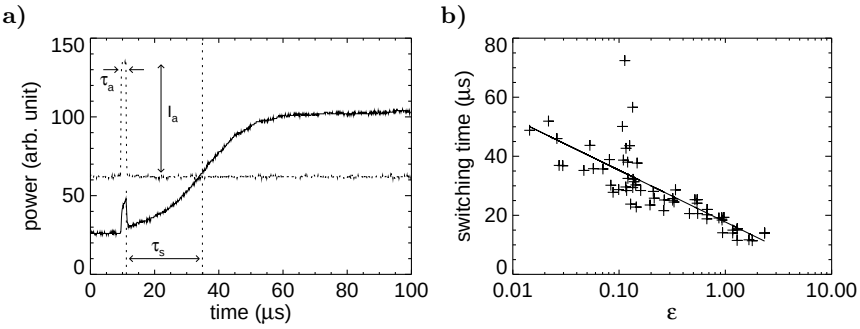

Fig. 25. a) Temporal evolution of transmitted power during ignition of a FS (solid line) after an addressing pulse is applied (dashed line). b) Distribution of switching times in dependence on the control parameter ϵ (see text). The spread in switching times which is apparent around $\epsilon \approx 0.1$ is probably related to perturbations of parameters. Parameter: $d = 70$ mm, $\Delta = 8.9$ GHz, $B_\perp = 2.35\,\mu$T, $B_z = 15.1\,\mu$T, cell temperature 313.2°C, $p_{N_2} = 200$ hPa, $P_{in} = 76$ mW (from [111]).

problem of the divergence at the separatrix always exists. For semiconductor systems, switching times in the nanosecond-range are found [88, 12, 90] after first experiments were limited by thermal time scales [85]. These investigations demonstrate clearly that the knowledge of unstable states can be very significant in understanding and control of spatial structures in nonlinear optical systems. This makes the analysis of stationary solutions an even more valuable technique in the study of model systems.

9 Conclusion

We have discussed a class of stable soliton-like structures predicted to exist in pattern-forming nonlinear optical systems containing any of a wide variety of nonlinear materials. This class includes semiconductor micro-resonators, which is promising for possible applications of these cavity and feedback solitons. They can be formed into two-dimensional arrays of information bits which can be written, stored, read, erased, and spatially manipulated in various ways. They can thus act as the basis of a new kind of all-optical parallel processor, with functionalities not available to other processing and storage devices in information technology.

Apart from this applicative aspect, their formation, stabilization and interaction involves a lot of interesting physics. Particularly intriguing is their 'quasi-particle' nature and their interaction properties. Although obviously numerous details remain to be worked out, these might open the intriguing possibility to construct a parallel to the chain of complexity known from equilibrium physics (atom – molecule/cluster - crystal/solid state lattice) in non-

equilibrium physics: single CS/FS – clusters/molecules – localized patterns – spatially extended periodic patterns.

Another intriguing aspect is the astonishing parallels between CS and FS in shape, bifurcation characteristics and interaction behavior. This illustrates that the existence of dissipation and feedback creates a universality transcending the differences in geometry between the two systems and that both should be regarded as representatives of the very general class of dissipative optical solitons. Nevertheless, it is of course instructive and important to understand and interpret the mechanism of localization in each specific system and we commented on several aspects of that.

10 Acknowledgements

This work is based on research which was partially supported by ESPRIT project 28235 PIANOS and EPSRC grant GR/M 19727. We thank our colleagues and collaborators for many helpful discussions and insights. We especially thank Andrew Scroggie for important contributions to this work. T.A. is grateful to Burkhard Schäpers and Wulfhard Lange for the fruitful collaboration on the subject. Their work was supported by the Deutsche Forschungsgemeinschaft.

References

1. N. N. Rosanov. *Transverse patterns in wide-aperture nonlinear optical systems.* Progress in Optics **XXXV**, 1–60 (1996).
2. L. A. Lugiato, M. Brambilla, and A. Gatti. *Optical pattern formation.* Adv. Atom. Mol. Opt. Phys. **40**, 229–306 (1999).
3. F. T. Arecchi, S. Boccaletti, and P. L. Ramazza. *Pattern formation and competition in nonlinear optics.* Phys. Rep. **318**, 1–83 (1999).
4. C. O. Weiss, M. Vaupel, K. Staliunas, G. Slekys, and V. B. Taranenko. *Solitons and Vortices in lasers.* Appl. Phys. B **68**, 151–168 (1999).
5. S. Trillo and W. E. Torruellas, editors. *Spatial Solitons*, volume 82 of *Springer Series in Optical Sciences.* Springer, Berlin (2001).
6. T. Ackemann and W. Lange. *Optical pattern formation in alkali metal vapors: Mechanisms, phenomena and use.* Appl. Phys. B **72**, 21–34 (2001).
7. W. J. Firth. *Theory of Cavity Solitons.* In A. D. Boardman and A. P. Sukhorukov, editors, *Soliton-Driven Photonics*, pages 459–485. Kluwer Academic Publishers, London (2001).
8. W. J. Firth and C. O. Weiss. *Cavity and feedback solitons.* Opt. Photon. News **13**(2), 54–58 (2002).
9. N. N. Rosanov. *Spatial hysteresis and optical patterns.* Springer Series in Synergetics. Springer, Berlin (2002).
10. U. Peschel, D. Michaelis, and C. O. Weiss. *Spatial solitons in optical cavities.* IEEE J. Quantum Electron. **39**, 51–64 (2003).

11. L. A. Lugiato. *Introduction to the feature section on cavity solitons: An overview.* IEEE J. Quantum Electron. **39**(2), 193–196 (2003).
12. C. O. Weiss. *This book.*
13. N. N. Rosanov. *This book.*
14. C. Etrich, U. Peschel, and F. Lederer. *Solitary Waves in Quadratically Nonlinear Resonators.* Phys. Rev. Lett. **79**, 2454–2457 (1997).
15. U. Peschel, D. Michaelis, C. Etrich, and F. Lederer. *Formation, motion, and decay of vectorial cavity solitons.* Phys. Rev. E **58**, R2745–R2748 (1998).
16. D. Michaelis, U. Peschel, C. Etrich, and F. Lederer. *Quadratic Cavity Solitons – The Up-Conversion Case.* IEEE J. Quantum Electron. **39**, 255–268 (2003).
17. S. Longhi. *Localized structures in optical parametric oscillation.* Physica Scripta **56**, 611–618 (1997).
18. K. Staliunas and V. J. Sánchez-Morcillo. *Localized structures in degenerate optical parametric oscillators.* Opt. Commun. **139**, 306–312 (1997).
19. G.-L. Oppo, A. J. Scroggie, and W. J. Firth. *From domain walls to localized structures in degenerate optical parametric oscillators.* J. Opt. B: Quantum Semiclass. Opt. **1**, 133–138 (1999).
20. M. Le Berre, D. Leduc, E. Ressayre, and A. Tallet. *Striped and circular domain walls in the DOPO.* J. Opt. B: Quantum Semiclass. Opt. **1**, 153–160 (1999).
21. D. V. Skryabin and W. J. Firth. *Interaction of cavity solitons in degenerate optical parametric oscillators.* Opt. Lett. **24**, 1056–1059 (1999).
22. M. Tlidi, M. Le Berre, E. Ressayre, A. Tallet, and L. Di Menza. *High-intensity localized structures in the degenerate optical parametric oscillator: Comparisom between the propagation and the mean-field model.* Phys. Rev. A **61**, 043806 (2000).
23. G. Izús, M. San Miguel, and M. Santagiustina. *Bloch domain walls in type II optical parametric oscillators.* Opt. Lett. **25**, 1454–6 (2000).
24. G. L. Oppo, A. J. Scroggie, and W. J. Firth. *Characterization, dynamics and stabilization of diffractive domain walls and dark ring cavity solitons in parametric oscillators.* Phys. Rev. E **63**, 066209 (2001).
25. C. Etrich, D. Michaelis, and F. Lederer. *Bifurcations, stability, and multistability of cavity solitons in parametric downconversion.* J. Opt. Soc. Am. B **19**, 792–801 (2002).
26. D. Gomila, P. Colet, M. San Miguel, A. Scroggie, and G. L. Oppo. *Stable droplets and dark-ring cavity solitons in nonlinear optical devices.* IEEE J. Quantum Electron. **39**, 238–244 (2003).
27. R. Vilaseca, M. C. Torrent, J. García-Ojalvo, E. Brambilla, and M. San Miguel. *Two-photon cavity solitons in active optical media.* Phys. Rev. Lett. **87**, 083902 (2001).
28. R. Gallego, M. San Miguel, and R. Toral. *Self-similar domain growth, localized structures, and labyrinthine patterns in vectorial Kerr resonators.* Phys. Rev. E **61**, 2241–4 (2000).
29. V. J. Sánchez-Morcillo, I. Pérez-Arjona, Silva F., G. J. Valcárcel, and E. Roldán. *Vectorial Kerr cavity solitons.* Opt. Lett. **25**, 957–959 (2000).
30. E. Große Westhoff, V. Kneisel, Yu. A. Logvin, T. Ackemann, and W. Lange. *Pattern formation in the presence of an intrinsic polarization instability.* J. Opt. B: Quantum Semiclass. Opt. **2**, 386–392 (2000).
31. V. B. Taranenko, K. Staliunas, and C. O. Weiss. *Pattern formation and localized structures in degenerate optical parametric mixing.* Phys. Rev. Lett. **81**, 2236–2239 (1998).

32. V. B. Taranenko, M. Zander, P. Wobben, and C. O. Weiss. *Stability of localized structures in degenerate wave mixing.* Appl. Phys. B **69**, 337–339 (1999).
33. M. Pesch, E. Große Westhoff, T. Ackemann, and W. Lange. Vectorial solitons and higher-order localized states in a single-mirror feedback system. In *Nonlinear Guided Waves and Their Applications.* Toronto, Canada, March 28-31,2004. Paper TuC24 (2004).
34. V. Yu. Bazhenov, V. B. Taranenko, and M. V. Vasnetsov. *Transverse optical effects in bistable active cavity with nonlinear absorber on bacteriorhodopsin.* Proc. SPIE **1840**, 183–193 (1992).
35. M. Saffman, D. Montgomery, and D. Z. Anderson. *Collapse of a transverse-mode continuum in a self-imaging photorefractively pumped ring resonator.* Opt. Lett. **19**, 518–520 (1994).
36. V. B. Taranenko, K. Staliunas, and C. O. Weiss. *Spatial soliton laser: localized structures in a laser with a saturable absorber in a self-imaging resonator.* Phys. Rev. A **56**, 1582–1591 (1997).
37. D. W. McLaughlin, J. V. Moloney, and A. C. Newell. *Solitary waves as fixed points of infinite-dimensional maps in an optical bistable ring cavity.* Phys. Rev. Lett. **51**, 75–78 (1983).
38. J. V. Moloney and A. C. Newell. *Nonlinear Optics.* Addison-Wesley, Redwood City (1992). Fig. 5.16, p. 225 and associated text.
39. H. M. Gibbs. *Optical Bistability: Controlling Light with Light.* Academic Press, Orlando (1985).
40. L. A. Lugiato. *Theory of optical bistability.* Progress in Optics XXI pages 70–216 (1984).
41. W. J. Firth and G. K. Harkness. *Cavity solitons.* Asian J. Phys. **7**, 665–677 (1998).
42. G. S. McDonald and W. J. Firth. *Spatial solitary-wave optical memory.* J. Opt. Soc. Am. B **7**, 1328–1335 (1990).
43. G. S. McDonald and W. J. Firth. *Switching dynamics of spatial solitary wave pixels.* J. Opt. Soc. Am. B **10**, 1081–1089 (1993).
44. N. N. Rosanov and G. V. Khodova. *Autosolitons in nonlinear interferometers.* Opt. Spectrosc. **65**, 449–450 (1988).
45. N. N. Rosanov and G. V. Khodova. *Diffractive autosolitons in nonlinear interferometers.* J. Opt. Soc. Am. B **7**(6), 1057–65 (1990).
46. W. J. Firth and I. Galbraith. *Diffusive transverse coupling of bistable elements - switching waves and crosstalk.* IEEE J. Quantum Electron. **21**, 1399–1403 (1985).
47. N. B. Abraham and W. J. Firth. *Overview of transverse effects in nonlinear-optical systems.* J. Opt. Soc. Am. B **7**, 951–961 (1990).
48. M. Kreuzer, H. Gottschilk, Th. Tschudi, and R. Neubecker. *Structure formation and self-organization phenomena in bistable optical elements.* Mol. Cryst. Liquid Cryst. **207**, 219–230 (1991).
49. R. Neubecker and T. Tschudi. *Self-induced mode as a building element of transversal pattern formation.* J. Mod. Opt. **41**, 885–906 (1994).
50. G. Giusfredi, J. F. Valley, R. Pon, G. Khitrova, and H. M. Gibbs. *Optical instabilities in sodium vapor.* J. Opt. Soc. Am. B **5**, 1181–1191 (1988).
51. L. A. Lugiato and R. Lefever. *Spatial dissipative structures in passive optical systems.* Phys. Rev. Lett. **58**, 2209–2211 (1987).

52. I. V. Barashenkov, N. V. Alexeeva, and E. V. Zemlyanaya. *Two- and three-dimensional oscillons in nonlinear Faraday resonance.* Phys. Rev. Lett. **89**, 104101 (2002).
53. P. B. Umbanhowar, F. Melo, and H. L. Swinney. *Localized excitations in a vertically vibrated granular layer.* Nature **382**, 793–796 (1996).
54. T. Maggipinto, M. Brambilla, G. K. Harkness, and W. J. Firth. *Cavity solitons in semiconductor microresonators: Existence, stability, and dynamical properties.* Phys. Rev. E **62**(6), 8726–8739 (2000).
55. G. K. Harkness, W. J. Firth, G. L. Oppo, and J. M. McSloy. *Computationally Determined Existence and Stability of Transverse Structures: I. Periodic Optical Patterns.* Phys. Rev. E **66**, 046605 (2002).
56. J. M. McSloy, W. J. Firth, G. L. Oppo, and G. K. Harkness. *Computationally Determined Existence and Stability of Transverse Structures: II. Multi-Peaked Cavity Solitons.* Phys. Rev. E **66**, 046606 (2002).
57. T. Maggipinto, M. Brambilla, and W. J. Firth. *Characterization of stationary patterns and their link with cavity solitons in semiconductor microresonators.* IEEE J. Quantum Electron. **39**, 206–215 (2003).
58. W. J. Firth, A. Lord, and A. J. Scroggie. *Optical bullet holes.* Phys. Scr. **T67**, 12–16 (1996).
59. W. J. Firth, G. K. Harkness, A. Lord, J. M. McSloy, D. Gomila, and P. Colet. *Dynamical properties of two-dimensional Kerr cavity solitons.* J. Opt. Soc. Am. B **19**(4), 747–752 (2002).
60. K. Staliunas. *Three-dimensional Turing structures and spatial solitons in optical parametric oscillators.* Phys. Rev. Lett. **81**, 81–84 (1998).
61. M. Tlidi and P. Mandel. *Three-dimensional optical crystals and localized structures in cavity second harmonic generation.* Phys. Rev. Lett. **83**, 4995–4998 (1999).
62. G. Steinmeyer, A. Schwache, and F. Mitschke. *Quantitative charakterization of turbulence in an optical experiment.* Phys. Rev. E **53**, 5399–5402 (1996).
63. S. Wabnitz. *Suppression of interactions in a phase-locked optical memory.* Opt. Lett. **18**, 601–603 (1993).
64. M. Tlidi, P. Mandel, and R. Lefever. *Localized structures and localized patterns in optical bistability.* Phys. Rev. Lett. **73**, 640–643 (1994).
65. W. J. Firth and A. J. Scroggie. *Optical bullet holes: robust controllable localized states of a nonlinear cavity.* Phys. Rev. Lett. **76**, 1623–1626 (1996).
66. W. J. Firth and A. J. Scroggie. *Spontaneous pattern formation in an absorptive system.* Europhys. Lett. **26**, 521–526 (1994).
67. T. Ackemann, S. Barland, J. R. Tredicce, M. Cara, S. Balle, R. Jäger, P. M. Grabherr, M. Miller, and K. J. Ebeling. *Spatial structure of broad-area vertical-cavity regenerative amplifiers.* Opt. Lett. **25**, 814–816 (2000).
68. P. Coullet, C. Riera, and C. Tresser. *Stable static localized structures in one dimension.* Phys. Rev. Lett. **84**, 3069–3072 (2000).
69. P. Coullet, C. Riera, and C. Tresser. *Qualitative theory of stable stationary localized structures in one dimension.* Prog. Theor. Phys. Suppl. **139**, 46–58 (2000).
70. Y. Pomeau. *Front motion, metastability and subcritical bifurcations in hydrodynamics.* Physica D **23**, 3–11 (1986).
71. A. G. Vladimirov, J. M. McSloy, D. V. Skryabin, and W. J. Firth. *Two-dimensional clusters of solitary structures in driven optical cavities.* Phys. Rev. E **65**, 046606 (2002).

72. W. J. Firth. *Optical Memory and Spatial Chaos.* Phys. Rev. Lett. **61**, 329–332 (1988).
73. P. Coullet, C. Riera, and C. Tresser. *A new approach to data storage using localized structures.* Chaos **14**, 193–198 (2004).
74. M. Tlidi and P. Mandel. *Spatial patterns in nascent optical bistability.* Chaos, Solitons & Fractals **4**, 1475–1486 (1994).
75. M. Brambilla, L. A. Lugiato, and M. Stefani. *Interaction and control of optical localized structures.* Europhys. Lett. **34**, 109–114 (1996).
76. M. Brambilla, L. A. Lugiato, F. Prati, L. Spinelli, and W. J. Firth. *Spatial soliton pixels in semiconductor devices.* Phys. Rev. Lett. **79**, 2042–2045 (1997).
77. L. Spinelli, G. Tissoni, M. Brambilla, F. Prati, and L. A. Lugiato. *Spatial solitons in semiconductor microcavities.* Phys. Rev. A **58**, 2542–2559 (1998).
78. M. Tlidi, M. Georgiou, and P. Mandel. *Transverse patterns in nascent optical bistability.* Phys. Rev. A **48**, 4605–4609 (1993).
79. M. C. Cross and P. C. Hohenberg. *Pattern formation outside of equilibrium.* Rev. Mod. Phys. **65**, 851–1112 (1993).
80. S. Hoogland, J. J. Baumberg, S. Coyle, J. Baggett, M. J. Coles, and H. J. Coles. *Self-organized patterns and spatial solitons in liquid-crystal microcavities*. Phys. Rev. A **66**, 055801 (2002).
81. G. Tissoni, L. Spinelli, M. Brambilla, I. Perrini, T. Maggipinto, and L. A. Lugiato. *Cavity solitons in bulk semiconductor microcavities: dynamical properties and control.* J. Opt. Soc. Am. B **16**, 2095–2105 (1999).
82. L. Spinelli, G. Tissoni, M. Tarenghi, and M. Brambilla. *First principle theory for cavity solitons in semiconductor microresonators.* Eur. Phys. J. D **15**, 257–266 (2001).
83. S. Barbay, J. Koehler, R. Kuszelewicz, T. Maggipinto, I. M. Perrini, and M. Brambilla. *Optical patterns and cavity solitons in quantum-dot microresonators.* IEEE J. Quantum Electron. **39**, 245–254 (2003).
84. D. Michaelis, U. Peschel, and F. Lederer. *Multistable localized structures and superlattices in semiconductor optical resonators.* Phys. Rev. A **56**, R3366–R3369 (1997).
85. V. B. Taranenko and C. O. Weiss. *Incoherent optical switching of semiconductor resonator solitons.* Appl. Phys. B **72**(7), 893–895 (2001).
86. S. Barland, J. R. Tredicce, M. Brambilla, L. A. Lugiato, S. Balle, M. Giudici, T. Maggipinto, L. Spinelli, G. Tissoni, T. Knödel, M. Miller, and R. Jäger. *Cavity solitons as pixels in semiconductors.* Nature **419**, 699–702 (2002).
87. V. B. Taranenko, C. O. Weiss, and B. Schäpers. *From coherent to incoherent hexagonal patterns in semiconductor resonators.* Phys. Rev. A **65**, 13812 (2002).
88. V. B. Taranenko, F. J. Ahlers, and K. Pierz. *Coherent switching of semiconductor resonator solitons.* Appl. Phys. B **75**, 75–77 (2002).
89. I. Ganne, G. Slekys, I. Sagnes, and R. Kuszelewicz. *Precursor forms of cavity solitons in nonlinear semiconductor microresonators.* Phys. Rev. E **66**, 066613 (2002).
90. X. Hachair, S. Barland, L. Furfaro, M. Giudici, S. Balle, J. Tredicce, M. Brambilla, T. Maggipinto, I. M. Perrini, G. Tissoni, and L. Lugiato. *Cavity solitons in broad-area vertical-cavity surface-emitting lasers below threshold.* Phys. Rev. A **69**, 043817 (2004).
91. A. J. Scroggie, J. M. McSloy, and W. J. Firth. *Self-Propelled Cavity Solitons in Semiconductor Microresonators.* Phys. Rev. E **66**, 036607 (2002).

92. L. Spinelli, G. Tissoni, L. Lugiato, and M. Brambilla. *Thermal effects and transverse structures in semiconductor microcavities with population inversion.* Phys. Rev. A **66**, 023817 (2002).
93. S. Barland, O. Piro, M. Giudici, J. R. Tredicce, and S. Balle. *Experimental evidence of van der PolFitzhughNagumo dynamics in semiconductor optical amplifiers.* Phys. Rev. E **68**, 036209 (2003).
94. P. Coullet, J. Lega, B. Houchmanzadeh, and J. Lajzerowics. *Breaking chirality in nonequilibrium systems.* Phys. Rev. Lett. **65**, 1352–1355 (1990).
95. D. Michaelis, U. Peschel, F. Lederer, D. V. Skryabin, and W. J. Firth. *Universal criterion and amplitude equation for a nonequilibrium Ising-Bloch transition.* Phys. Rev. E **63**, 066602 (2001).
96. D. V. Skryabin, A. Yulin, D. Michaelis, W. J. Firth, G.-L. Oppo, U. Peschel, and F. Lederer. *Perturbation theory for domain walls in the parametric Ginzburg-Landau equation.* Phys. Rev. E **64**, 056618 (2001).
97. C. Degen, I. Fischer, W. Elsäßer, L. Fratta, P. Debernardi, G. Bava, M. Brunner, R. Hövel, M. Moser, and K. Gulden. *Transverse modes in thermally detuned oxide-confined vertical-cavity surface-emitting lasers.* Phys. Rev. A **63**, 23817 (2001).
98. T. Rössler, R. A. Indik, G. K. Harkness, and J. V. Moloney. *Modeling the interplay of thermal effects and transverse mode behavior in native-oxide confined vertical-cavity surface-emitting lasers.* Phys. Rev. A **58**, 3279–3292 (1998).
99. M. Bode. *Pattern formation in dissipative systems: A particle approach.* Adv. in Solid State Phys. **41**, 369–381 (2001).
100. H. U. Bödeker, M. C. Röttger, A. W. Liehr, Frank. T. D., R. Friedrich, and H. G. Purwins. *Noise-covered drift bifurcation of dissipative solitons in a planar gas-discharge system.* Phys. Rev. E **67**, 056220 (2003).
101. W. J. Firth. *Spatial instabilities in a Kerr medium with single feedback mirror.* J. Mod. Opt. **37**, 151–153 (1990).
102. G. D'Alessandro and W. J. Firth. *Spontaneous hexagon formation in a nonlinear optical medium with feedback mirror.* Phys. Rev. Lett. **66**, 2597–2600 (1991).
103. G. D'Alessandro and W. J. Firth. *Hexagonal spatial pattern for a Kerr slice with a feedback mirror.* Phys. Rev. A **46**, 537–548 (1992).
104. M. Kreuzer, A. Schreiber, and B. Thüring. *Evolution and switching dynamics of solitary spots in nonlinear optical feedback systems.* Mol. Cryst. Liq. Cryst. **282**, 91–105 (1996).
105. A. Schreiber, M. Kreuzer, B. Thüring, and T. Tschudi. *Experimental investigation of solitary structures in a nonlinear optical feedback system.* Opt. Commun. **136**, 415–418 (1997).
106. B. A. Samson and M. A. Vorontsov. *Localized states in a nonlinear optical system with a binary-phase slice and a feedback mirror.* Phys. Rev. A **56**, 1621–1626 (1997).
107. B. Schäpers, M. Feldmann, T. Ackemann, and W. Lange. *Interaction of localized structures in an optical pattern forming system.* Phys. Rev. Lett. **85**, 748–751 (2000).
108. P. L. Ramazza, S. Ducci, S. Boccaletti, and F. T. Arecchi. *Localized versus delocalized patterns in a nonlinear optical interferometer.* J. Opt. B: Quantum Semiclass. Opt. **2**(3), 399–405 (2000).

109. M. G. Clerc, S. Residori, and C. S. Riera. *First-order Frédericksz transition in the presence of light-driven feedback in nematic liquid cyrstals.* Phys. Rev. E **63**, 060701(R) (2001).
110. B. Schäpers, T. Ackemann, and W. Lange. *Characteristics and possible applications of localized structures in an optical pattern–forming system.* Proc. SPIE **4271**, 130–137 (2001).
111. B. Schäpers, T. Ackemann, and W. Lange. *Robust control of switching of localized structures and its dynamics in a single-mirror feedback scheme.* J. Opt. Soc. Am. B **19**(4), 707–715 (2002).
112. P. L. Ramazza, E. Benkler, U. Bortolozzo, S. Boccaletti, S. Ducci, and F. T. Arecchi. *Taloiring the profile and interactions of optical localized structures.* Phys. Rev. E **65**, 066204 (2002).
113. B. Gütlich, M. Kreuzer, R. Neubecker, and T. Tschudi. *Manipulation of solitary structures in a nonlinear optical single feedback experiment.* Mol. Cryst. Liq. Cryst. **375**, 281–289 (2002).
114. B. Schäpers, T. Ackemann, and W. Lange. *Properties of feedback solitons in a single-mirror experiment.* IEEE J. Quantum Electron. **39**(2), 227–237 (2003).
115. B. Gütlich, R. Neubecker, M. Kreuzer, and T. Tschudi. *Control and manipulation of solitary structures in a nonlinear optical single feedback experiment.* Chaos **13**, 239–246 (2003).
116. S. Rankin, E. Yao, and F. Papoff. *Traveling waves and counterpropagating bright droplets as a result of tailoring the transverse dispersion relation in a multistable optical system.* Phys. Rev. A **68**, 013821 (2003).
117. W. H. F. Talbot. *Facts relating to optical science. No. IV.* Philos. Mag. **9**(Third series), 401–407 (1836).
118. E. Ciaramella, M. Tamburrini, and E. Santamato. *Talbot assisted hexagonal beam patterning in a thin liquid crystal film with a single feedback mirror at negative distance.* Appl. Phys. Lett. **63**, 1604–1606 (1993).
119. T. Ackemann, B. Giese, B. Schäpers, and W. Lange. *Investigation of pattern forming mechanisms by Fourier filtering: properties of hexagons and the transition to stripes in an anisotropic system.* J. Opt. B: Quantum Semiclass. Opt. **1**, 70–76 (1999).
120. S. G. Odoulov, M. Yu. Goulkov, and O. A. Shinkarenko. *Threshold behavior in formation of optical hexagons and first order optical phase transition.* Phys. Rev. Lett. **83**, 3637–3640 (1999).
121. S. A. Akhmanov, M. A. Vorontsov, V. Yu. Ivanov, A. V. Larichev, and N. I. Zheleynykh. *Controlling transverse-wave interactions in nonlinear optics: generation and interaction of spatiotemporal structures.* J. Opt. Soc. Am. B **9**, 78–90 (1992).
122. A. Kastler. *Optical methods of atomic orientation and of magnetic resonance.* J. Opt. Soc. Am. **47**, 460–465 (1957).
123. F. Mitschke, R. Deserno, W. Lange, and J. Mlynek. *Magnetically induced optical self-pulsing in a nonlinear resonator.* Phys. Rev. A **33**, 3219–3231 (1986).
124. T. Ackemann, A. Heuer, Yu. A. Logvin, and W. Lange. *Light-shift induced level crossing and resonatorless optical bistability in sodium vapor.* Phys. Rev. A **56**, 2321–2326 (1997).
125. D. N. Maywar, G. P. Agrawal, and Y. Nakano. *Robust optical control of an optical-amplifier-based flip-flop.* Opt. Express **6**, 75–80 (2000).

126. W. Lange, Yu. A. Logvin, and T. Ackemann. *Spontaneous optical patterns in an atomic vapor: observation and simulation.* Physica D **96**, 230–241 (1996).
127. B. Schäpers. *Lokalisierte Strukturen in einem atomaren Dampf mit optischer Rückkopplung.* Phd thesis, Westfälische Wilhelms-Universität Münster (2001).
128. M. Kreuzer. *Grundlagen und Anwendungen von Füssigkristallen in der optischen Informations- und Kommunikationstechnologie.* PhD thesis, Darmstadt (1994).
129. T. Ackemann (2002). Unpublished.
130. G. Grynberg, A. Petrossian, M. Pinard, and M. Vallet. *Phase-contrast mirror based on four-wave mixing.* Europhys. Lett. **17**, 213 (1992).
131. G. Grynberg. *Roll and hexagonal patterns in a phase-contrast oscillator.* J. Phys. III **3**, 1345–1355 (1993).
132. M. Tlidi, A. G. Vladimirov, and P. Mandel. *Interaction and Stability of Periodic and Localized Structures in Optical Bistable Systems.* IEEE J. Quantum Electron. **39**, 216–226 (2003).
133. Yu. A. Logvin, B. Schäpers, and T. Ackemann. *Stationary and drifting localized structures near a multiple bifurcation point.* Phys. Rev. E **61**, 4622–4625 (2000).
134. S. Mêtens, G. Dewel, P. Borckmanns, and R. Engelhardt. *Pattern selection in bistable systems.* Europhys. Lett. **37**, 109–114 (1997).
135. W. J. Firth. *Processing Information with Arrays of Spatial Solitons.* Proc. SPIE **4016**, 388–394 (2000).
136. E. Lugagne Delpon, J. L. Oudar, and H. Lootvoet. *Operation of a* 4×1 *optical register as a fast access optical buffer memory.* Electron. Lett. **33**, 1161–1162 (1997).
137. P. Mandel. *Scaling properties of switching pulses.* Opt. Commun. **55**, 293–296 (1985).
138. B. Segard, J. Zemmouri, and B. Macke. *Noncritical slowing down in optical bistability.* Opt. Commun. **63**, 339–343 (1987).
139. J. Y. Bigot, A. Daunois, and P. Mandel. *Slowing down far from the limit points in optical bistability.* Phys. Lett. A **123**, 123–127 (1987).
140. F. Mitschke, C. Boden, W. Lange, and P. Mandel. *Exploring the dynamics of the unstable branch of bistable systems.* Opt. Commun. **71**, 385–392 (1989).